Synaptotagmin increases the dynamic range of synapses by driving Ca^{2+} - evoked release and by clamping a near-linear remaining Ca^{2+} sensor

Olexiy Kochubey, Ralf Schneggenburger

Laboratory of Synaptic Mechanisms, Brain-Mind Institute, École Polytechnique Fédérale de Lausanne, 1015 Lausanne, Switzerland

Running title: Release triggering and clamping function of Syt2

Keywords:

Calyx of Held • transmitter release • presynaptic protein • protein overexpression • asynchronous release • structure - function analysis

correspondence:
Ralf Schneggenburger (ralf.schneggenburger@epfl.ch)
Laboratory of Synaptic Mechanisms
École Polytechnique Fédérale de Lausanne (EPFL), Brain Mind Institute
1015 Lausanne, Switzerland
Fax +41 21 693 5350

Ca^{2+}-evoked transmitter release shows a high dynamic range over spontaneous release. We investigated the role of the Ca^{2+} sensor protein, Synaptotagmin-2 (Syt2), in both spontaneous and Ca^{2+} - evoked release under direct control of presynaptic $[Ca^{2+}]_i$, using a novel *in-vivo* rescue approach at the calyx of Held. Re-expression of Syt2 rescued the highly Ca^{2+} cooperative release, and suppressed the elevated spontaneous release seen in Syt2 KO synapses. This release clamping function was partially mediated by the poly-lysine motif of the C_2B domain. Using an aspartate mutation in the C_2B domain (D364N) in which Ca^{2+} triggering was abolished but release clamping remained intact, we show that Syt2 strongly suppresses the action of another, near-linear Ca^{2+} sensor that mediates release over a wide range of $[Ca^{2+}]_i$. Thus, Syt2 increases the dynamic range of synapses by driving release with a high Ca^{2+} cooperativity, as well as by suppressing a remaining, near-linear Ca^{2+} sensor.

Transmitter release at synapses is mediated by docked, and readily-releasable vesicles in the process of SNARE - dependent membrane fusion (Chen and Scheller, 2001; Jahn et al., 2003), which is intricately regulated by the intracellular Ca^{2+} concentration, $[Ca^{2+}]_i$, in the nerve terminal. Measurements at the calyx of Held, a large CNS synapse where presynaptic $[Ca^{2+}]_i$ can be controlled directly, have shown that brief local $[Ca^{2+}]_i$ elevations in the range of 10 - 40 µM drive transmitter release during an action potential (AP) (Bollmann et al., 2000; Schneggenburger and Neher, 2000; Wang et al., 2008; Kochubey et al., 2009). The fast phase of release is highly non-linearly regulated by Ca^{2+}, giving rise to a forth-power relationship between release and the local $[Ca^{2+}]_i$ (Dodge and Rahamimoff, 1967; Bollmann et al., 2000; Schneggenburger and Neher, 2000). On the other hand, at the resting $[Ca^{2+}]_i$ of nerve terminals, the rate of spontaneous release is about one-millionfold lower than the peak release rate during an AP, and this spontaneous release has a low Ca^{2+} cooperativity (Lou et al.,

2005). Thus, there is a large dynamic range of Ca^{2+} - evoked release as compared to the spontaneous release rate, but the underlying mechanisms are not well understood.

Synaptotagmins (Syts) are double C2 domain proteins, and Synaptotagmin1 is the Ca^{2+} sensor for fast release in many synapses, as revealed by knock-out studies in mice (Geppert et al., 1994; Stevens and Sullivan, 2003; Nishiki and Augustine, 2004; Maximov and Südhof, 2005) and Drosophila (Yoshihara and Littleton, 2002). In mammals, there are more than 15 Syt isoforms, and the closest homologue of Syt1 is Syt2 (Pang and Südhof, 2010). Both isoforms are expressed differentially in brain, with a dominant expression of Syt2 in the hindbrain and spinal cord (Geppert et al., 1991; Marqueze et al., 1995; Pang et al., 2006a). Syt2 is the Ca^{2+} sensor for fast release at the calyx of Held since Syt2, but not Syt1 is expressed at calyces (Pang et al., 2006b; Fox and Sanes, 2007; Xiao et al., 2010), and because fast release is strongly reduced at the calyx of Held synapse of Syt2 KO mice (Sun et al., 2007). Thus, Syt1 and Syt2 are Ca^{2+} sensors for transmitter release with a differential distribution between forebrain and hindbrain, but with similar functions.

Interestingly, deletion of Syt1 or Syt2 also leads to an increased spontaneous release in many preparations (Littleton et al., 1994; Pang et al., 2006b; Kerr et al., 2008; Xu et al., 2009; Chicka et al., 2008; Liu et al., 2009). This indicates that in addition to mediating Ca^{2+} - evoked release, Syt1/2 has a release clamping function (Yoshihara et al., 2003). Related to release clamping, it was found that in Syt1 KO synapses, the asynchronous release phase was enhanced (Nishiki and Augustine, 2004; Maximov and Südhof, 2005; Yoshihara and Littleton, 2002). In Ca^{2+} uncaging experiments at calyx synapses of Syt2 KO mice, slow Ca^{2+} - evoked release also remained, which was thought to represent the activity of a specific second Ca^{2+} sensor for asynchronous release (Sun et al., 2007). However, it is difficult to extrapolate from the remaining release in Syt1/2 KO synapses to a possible contribution of

alternative Ca^{2+} sensor(s) to asynchronous release in wild-type synapses. This is because in Syt1/2 KO synapses, atypical Ca^{2+} sensor(s) not present normally might gain access to the release apparatus (see discussion in Groffen et al., 2010). Alternatively, even if a second Ca^{2+} sensor is present normally, it might be suppressed by the release clamping function of Syt1/2. Therefore, it would be useful to molecularly isolate the release triggering- and release clamping functions of Syt1/2, and to study these functions separately in a synapse which enables the direct control of presynaptic $[Ca^{2+}]_i$.

Here, we have investigated the interaction of Syt2 with the remaining Ca^{2+} sensor(s) in a structure-function analysis of Syt2 at the calyx of Held synapse. Due to its large presynaptic nerve terminal, this synapse allows direct control of presynaptic $[Ca^{2+}]_i$ via Ca^{2+} uncaging techniques and loading with Ca^{2+} chelators (Bollmann et al., 2000; Schneggenburger, 2000; Lou et al., 2005). To study the role of specific Syt2 residues in controlling Ca^{2+} - triggering and release clamping, we have established an *in-vivo* rescue approach at the calyx of Held of Syt2 KO mice (Pang et al., 2006a), based on virus-mediated expression of proteins at the calyx of Held (Wimmer et al., 2004; Young and Neher, 2009). We show that Syt2, via the poly-lysine motif in its C_2B domain, clamps spontaneous- and slow Ca^{2+} - evoked release by suppressing the action of a surprisingly linear Ca^{2+} sensor which remained in the Syt2 KO synapses. The results show an intricate regulation of both spontaneous, and Ca^{2+}-evoked release by Syt2.

Results

In-vivo expression leads to correct targeting of Syt2 at the calyx of Held

We wished to perform a mutational analysis of the function of Syt2 at the calyx of Held, in the absence of confounding effects of remaining wild-type Syt2 protein. For this purpose, we established functional rescue of Ca^{2+}-evoked transmission in Syt2 KO mice (Sun et al., 2007),

using virus-mediated *in-vivo* expression of Syt2. We used a second-generation adenovirus vector, which drove the expression of two proteins (eGFP and a Syt2 construct) under two separate human Synapsin-1 promotors (hSyn; Young and Neher, 2009; Kügler et al., 2003; see Experimental Procedures). We first analyzed by immunohistochemistry how the recombinant Syt2 protein is targeted to calyces of Held, following stereotactic injection of an adenovirus (ad: hSyn-Syt2^{WT}: hSyn-eGFP virus) into the ventral cochlear nucleus (VCN) of a Syt2 KO mouse. Fig. 1A shows numerous calyceal terminals with both GFP and Syt2 immunofluorescence in the MNTB contralateral to the injection site, reflecting the successful transduction of a large number of globular bushy cells in the VCN, which give rise to calyces of Held (see Cant and Benson, 2003, and references therein). In high-resolution confocal images (Fig. 1B), eGFP was localized both in calyces and in adjacent axonal fibers (Fig. 1B, arrows); this was expected because eGFP is a diffusible protein. In contrast, the anti-Syt2 signal was limited to the ring-shaped, calyceal nerve terminals (Fig. 1B, arrowheads). This shows that exogenously expressed Syt2 is properly targeted to the calyx of Held terminals, without remaining at large concentrations in the axonal compartments.

We next estimated the concentration of overexpressed Syt2 relative to the endogenous protein levels in wild-type calyces, by performing quantitative confocal immunohistochemistry (Fig. 1C-F). We compared confocal images of brainstem sections of a Syt2 KO mouse expressing the Syt2^{WT} - eGFP construct (Fig. 1C), with those of a sham-injected wild-type mouse (Fig. 1D). We found that the Syt2 signal of calyces in the Syt2 KO mouse in which Syt2 was re-expressed (Fig. 1C, right) was brighter than the Syt2 signal from the wild-type mouse (Fig. 1D, right). A quantitative analysis showed that calyces overexpressing Syt2 in a Syt2 KO mouse had a significantly higher Syt2 signal (603 ± 295 a.u.; n = 218 calyces) than calyces in the sham-injected wild-type mouse (194 ± 268 a.u.; n = 177 calyces; $p < 0.001$; Fig. 1F). As expected, calyces of Syt2 KO mice that were eGFP-negative and therefore not transduced

(Fig. 1C, arrowhead) did not show a detectable Syt2 signal (Fig. 1F). All three types of calyces had comparable VGluT2 signal intensities (Fig. 1E). Thus, quantitative immunohistochemistry shows that recombinant Syt2 is present at an approximately three-fold higher concentration in the nerve terminal as compared to the endogenous protein.

***In-vivo* expression of Syt2 fully rescues Ca^{2+}-evoked release and release clamping**

Genetic deletion of Syt2 in KO mice led to severe impairment of Ca^{2+}-evoked release at the calyx of Held (Sun et al., 2007). We next investigated whether virus-mediated expression of $Syt2^{WT}$ can functionally rescue the release phenotype at the calyx of Held synapse in Syt2 KO mice. We used Ca^{2+} uncaging which allowed us to relate the transmitter release rates directly to the $[Ca^{2+}]_i$ step in the nerve terminal (Schneggenburger and Neher, 2000; Bollmann et al., 2000). To establish control values for the rescue experiments, we first investigated Ca^{2+}-evoked release in wild-type and Syt2 KO synapses of P12 - P15 mice expressing eGFP alone (Fig. 2A, B). Ca^{2+} uncaging, which produced a $[Ca^{2+}]_i$ elevation to 6.8 µM in a Syt2 wild-type synapse triggered a fast EPSC of 22.3 nA amplitude (Fig. 2A1), corresponding to a peak release rate of ~ 950 ves/ms as analyzed by EPSC deconvolution (Fig. 2A1, bottom). In contrast, in a calyx of Held synapse from a Syt2 KO mouse, there was only a small, slowly rising EPSC (~ 0.2 nA, Fig. 2B1) with a peak release rate of ~ 2 ves/ms, despite the fact that Ca^{2+} uncaging produced a $[Ca^{2+}]_i$ step of 9.3 µM amplitude. On average, the peak release rates in response to $[Ca^{2+}]_i$ steps to 7 - 20 µM were reduced by ~ 500 - fold in Syt2 KO mice (Fig. 2D). This effect of genetic removal of Syt2 is somewhat stronger than what was reported previously in younger Syt2 KO mice (Sun et al., 2007; see Discussion). We also observed that the mEPSC frequency was higher in Syt2 KO synapses (Fig. 2B2; 19.5 ± 3.4 Hz, n = 10) than in wild-type synapses (Fig. 2A2; 1.74 ± 0.54 Hz; n = 5; $p < 0.001$). Importantly, however the basal $[Ca^{2+}]_i$ was unchanged between Syt2 KO synapses (48.0 ± 5.6 nM; n = 8) and wild-type

synapses (44.2 ± 2.9 nM; n = 8; Fig. S1), showing that the elevated mEPSC frequency was not caused by a mis-regulation of the basal presynaptic $[Ca^{2+}]_i$ in Syt2 KO mice.

We next asked whether expression of wild-type Syt2 ($Syt2^{WT}$ + eGFP construct) in calyces of Held can rescue Ca^{2+} - evoked release in Syt2 KO synapses. In $Syt2^{WT}$ rescue calyces, Ca^{2+} uncaging evoked large and fast EPSCs, with a peak release rate of ~ 1000 ves/ms in the example of Fig. 2C1. The average release rate in $Syt2^{WT}$ rescue synapses was 981 ± 326 ves/ms in the range of 7 - 20 µM $[Ca^{2+}]_i$ (n = 16 flash responses from n = 4 pairs). This value was not significantly different from the peak release rate in wild-type synapses (1260 ± 220 ves/ms; p = 0.47; Fig. 2D), but it was ~ 500 -fold larger than the release rate in synapses from Syt2 KO mice expressing eGFP alone (see above; 2.4 ± 0.8 ves/ms; n = 14 flashes in 7 pairs; Fig. 2D, red symbols).

When we plotted the release rate over a wide range of $[Ca^{2+}]_i$ (~ 1 - 70 µM), the control data of wild-type synapses expressing eGFP, and the rescue data from calyces in Syt2 KO mice expressing $Syt2^{WT}$ and eGFP overlaid well (Fig. 2F, grey and black data points, respectively). On the other hand, the Syt2 KO synapses showed a very shallow Ca^{2+} - dependency, which was fitted by a line with a slope of 1.1 in double-logarithmic coordinates. Thus, vesicles in the absence of Syt2 are released with a much lower efficiency and Ca^{2+} cooperativity than in the wild-type mice, but the deficient Ca^{2+} triggering is fully rescued by expression of Syt2 (Fig. 2F, black data points). Similarly, in a plot of the release delay as a function of $[Ca^{2+}]_i$ (Fig. 2G), the Syt2 KO data showed an about 8-10 fold longer delay, and Syt2 expression completely rescued the fast release delays observed in the wild-type synapses (Fig. 2G, compare grey and black data points). Thus, *in-vivo* virus-mediated expression of Syt2 fully rescues the amount, and the kinetics of Ca^{2+}-evoked release in calyces of Syt2 KO mice.

Importantly, Syt2 expression also suppressed the elevated mEPSC frequency observed in Syt2 KO synapses (Fig. 2C2). In Syt2 rescue synapses, the mEPSC frequency was low (1.0 ± 0.2 Hz; n = 12), and not significantly different from wild-type synapses (p = 0.23; Fig. 2E). This suggests that Syt2 has a specific role in suppressing spontaneous release, which we will refer to as the 'release clamping' function of Syt2 (Littleton et al., 1994).

Ca^{2+}-evoked release and release clamping depend on different structural elements in the C_2B domain of Syt2

Having established an efficient *in-vivo* rescue of both the Ca^{2+}-evoked release and of release clamping, we are now in a position to perform a structure-function analysis of Syt2 under direct control of presynaptic $[Ca^{2+}]_i$ at the calyx of Held. We decided to assess the role of specific residues in the C_2B domain of Syt2, because the C_2B domain has been shown to be critically important for Ca^{2+}-evoked release in Syt1 (Desai et al., 2000; Mackler et al., 2002; Robinson et al., 2002; Nishiki and Augustine, 2004). In addition, the C_2B domain shows Ca^{2+} independent binding to the t-SNAREs (Rickman et al., 2004; Rickman et al., 2006), and could therefore be involved both in Ca^{2+} triggering of release, as well as in the release clamping function of Syt2.

We first studied the effect of removing the entire C_2B domain of Syt2 (see Fig. 3G for a scheme of the mutations used here). This mutant ($Syt2^{\Delta C2B}$) showed only little rescue of Ca^{2+}-evoked release (Fig. 3A1; Fig. 3E, open bar), and the spontaneous mEPSC frequency remained high (Fig. 3A2; 13.4 ± 3.6 Hz, n = 5 cells; see Fig. 3F, open bar). This suggests that the C_2B domain is essential for Ca^{2+}-evoked release (Yoshihara and Littleton, 2002; Mackler et al., 2002; Nishiki and Augustine, 2004) as well as for release clamping.

We next investigated single point mutations in the C_2B domain to isolate residues involved in triggering Ca^{2+} - dependent release, and in release clamping. The negatively charged Ca^{2+}

coordination sites in the C_2B domain of Syt are critically important for Ca^{2+}-evoked release (Mackler et al., 2002; Nishiki and Augustine, 2004), but it is unclear whether release clamping involves similar structural elements as those involved in Ca^{2+}-evoked release. Therefore, we neutralized the third aspartate residue to asparagine (Syt2 D364N; called $Syt2^{D3}$ mutant), and asked whether this mutation differentially affects Ca^{2+}-evoked release, and the clamping of spontaneous release. Expression of the $Syt2^{D3}$ construct in calyces from Syt2 KO mice was completely inefficient in rescuing Ca^{2+}-evoked release (Fig. 3B1). Indeed, the average peak release rate of Ca^{2+}-evoked release was even lower (0.33 ± 0.14 ves/ms) than the one observed in Syt2 KO calyces (2.4 ± 0.8 ves/ms, Fig. 3E; compare blue bar, and open red bar respectively; $p = 0.022$). On the other hand, the mEPSC frequency following rescue with $Syt2^{D3}$ was low (Fig. 3B2), with an average value of 1.25 ± 0.45 Hz, indistinguishable from rescue with $Syt2^{WT}$ (Fig. 3F, compare blue and black bar; $p = 0.66$). This shows that the $Syt2^{D3}$ site is critically involved in mediating Ca^{2+} - evoked release; the $Syt2^{D3}$ mutation even has a dominant-negative effect on the remaining Ca^{2+} - evoked release in Syt2 KO synapses (Fig. 3E; Nishiki and Augustine, 2004). On the other hand, the clamping of spontaneous release is intact in the $Syt2^{D3}$ mutant. Thus, it is possible that release clamping acts on both spontaneous release and on the remaining Ca^{2+} - evoked release in the absence of Syt2; a possibility that will be addressed in more detail below (Figs. 4, 5).

We next wished to study structural elements involved in the clamping of spontaneous release. We tested whether the conserved poly-lysine motif of the Syt2 C_2B domain, which mediates Ca^{2+}-independent binding of Syt1 to the syntaxin-1/SNAP-25 t-SNARE dimer (Rickman et al., 2004; Rickman et al., 2006), could be involved in the suppression of spontaneous release. We introduced a triple lysine-to-glutamine substitution (Syt2 K327Q, K328Q, K332Q; called $Syt2^{3K}$), since this mutant has no residual binding to the t-SNARE dimer (Rickman et al., 2004) and induced increased spontaneous release at the Drosophila NMJ (Mackler and Reist,

2001). In Syt2^{3K} rescue synapses, $[Ca^{2+}]_i$ steps to around 10 μM caused large and fast EPSCs (Fig. 3C1), suggesting efficient rescue of fast Ca^{2+}-evoked release. On average, the peak release rate in the range of 7 - 20 μM $[Ca^{2+}]_i$ was 819 ± 99 ves/ms (n = 10 synapses; Fig. 3E, green bar), not significantly different from the Syt2^{WT} rescue (Fig. 3E, black bar; p = 0.07). Similarly, in plots of the peak release rates and the synaptic delays as a function of $[Ca^{2+}]_i$, the data obtained with the Syt2^{3K} mutant were indistinguishable from the rescue with the Syt2^{WT} construct, and from the wild-type data (Fig. S2), indicating a near-complete rescue of the intrinsic Ca^{2+} - sensitivity of release by Syt2^{3K}. Nevertheless, expressing Syt2^{3K} did not fully rescue release in response to short presynaptic depolarizations (Fig. S2). This indicates that the poly-lysine site of the C_2B domain contributes to localize vesicles close to Ca^{2+} channels, a new role of Syt2 which has been identified recently using a more C-terminal mutation in the C_2B domain (Young and Neher, 2009).

Importantly, while the Syt2^{3K} mutant could fully rescue the intrinsic Ca^{2+} sensitivity of release (Fig. 3C1), the mEPSC frequency at rest was still elevated (8.3 Hz in the example of Fig. 3C2), indicating incomplete clamping of spontaneous release by Syt2^{3K} mutant. On average, the mEPSC frequency was 6.7 ± 2.1 Hz in the Syt2^{3K} rescue, significantly higher than in the rescue with Syt2^{WT} (p = 0.016), but somewhat lower than in the Syt2 KO (p = 0.004; Fig. 3F, green bar). These results show that the poly-lysine motif of the C_2B domain is involved in clamping of spontaneous release, but not in triggering fast Ca^{2+}-dependent release *per se* (see also Discussion).

Finally, we combined the mutations of the poly-lysine motif and the Ca^{2+}-binding site in a quadruple mutation (K327Q, K328Q, K332Q / D364N) referred to as Syt2$^{3K/D3}$. We expected to observe synapses with very little Ca^{2+} - evoked release but with a high mEPSC frequency. Indeed, Ca^{2+} uncaging did not trigger fast release within the first 50 ms following the flash in

many cases (Fig. 3D1), whereas release clamping was only partially supported, since the mEPSC frequency was high (Fig. 3D2). On average, Syt2$^{3K/D3}$ revealed low Ca^{2+}-evoked release rates (0.90 ± 0.33 ves/ms; Fig. 3E, purple bar), similar to the value for the Syt2^{D3} mutant, and ~ 2.5-fold lower than in Syt2 KO synapses, although this latter comparison did not reach statistical significance (Fig. 3E, compare purple and open red bar respectively; p = 0.098). The mEPSC frequency was 7.9 ± 1.5 Hz, similar to the one observed in the poly-lysine stretch mutation alone (Fig. 3F, compare purple and green bar; p = 0.65). Therefore, synapses rescued with the Syt2$^{3K/D3}$ construct showed a combination of the effects of the two independent Syt2^{D3} and Syt2^{3K} mutants: neither Ca^{2+}-evoked release, nor spontaneous release clamping were supported effectively.

The Ca^{2+} sensitivity of spontaneous release

Syt2 is responsible for triggering Ca^{2+}-evoked release, but at the same time it clamps spontaneous release, a function which at least partially depends on the poly-lysine motif in the C_2B domain (Fig. 3). It has remained controversial, however, whether unclamped spontaneous release is simply caused by a low rate of Ca^{2+} - independent vesicle fusion (Chicka et al., 2008), or else, whether spontaneous release is Ca^{2+} dependent as found in a recent study (Xu et al., 2009).

To test whether the elevated mEPSC frequency in Syt2 KO synapses is Ca^{2+} - dependent, we loaded the Ca^{2+} chelator BAPTA via presynaptic whole-cell recordings into calyces of Syt2 KO mice. The mEPSC frequency was high as long as the presynaptic pipette was in the cell-attached mode, with a temporal average of ~ 33 Hz in the example of Fig. 4A. After establishing presynaptic whole-cell recording with a 10 mM BAPTA / 0 Ca^{2+} pipette solution, the mEPSC frequency was strongly suppressed within about a minute (Fig. 4A, arrowhead). On average, the mEPSC frequency was reduced from 23.4 ± 6.1 Hz before presynaptic whole-

cell recording, to 1.5 ± 0.15 Hz following the loading with 10 mM BAPTA (Fig. 4B, n = 4 synapses, p = 0.012, paired t-test). This indicates that the spontaneous release in Syt2 KO mice is driven by Ca^{2+}.

We then wished to use EGTA to consolidate the findings with presynaptic BAPTA loading. EGTA has a similarly high affinity for Ca^{2+} as BAPTA, but has a much lower on-rate for Ca^{2+} binding (Adler et al., 1991; Neher, 1998). Surprisingly, presynaptic whole-cell recording with 10 mM EGTA / 0 Ca^{2+} decreased the elevated mEPSC frequency in Syt2 KO calyces only modestly (Fig. 4B), despite the fact that the spatially averaged $[Ca^{2+}]_i$ in the nerve terminal, which we monitored with fura-2 Ca^{2+} imaging, was similarly low with BAPTA and EGTA (< 10 nM $[Ca^{2+}]_i$; see Fig. A, B; upper panels). On average, EGTA reduced the mEPSC frequency by only ~ 20%, an effect which was nevertheless significant (p = 0.024, paired t-test; Fig. 4D). An explanation for the differential blocking efficiency of BAPTA and EGTA is that spontaneous release in the Syt2 KO synapses results from short-lived Ca^{2+} transients, which can only be suppressed efficiently by BAPTA because of its faster on-rate of Ca^{2+} binding as compared to EGTA. Interestingly, removing extracellular Ca^{2+} or blocking voltage-gated Ca^{2+} channels with 0.2 mM Cd^{2+} did not affect the mEPSC frequency (Fig. S3). Therefore, it seems that the elevated mEPSC frequency in Syt2 KO synapses was caused by a local, probably intracellular Ca^{2+} source (Llano et al., 2000; Emptage et al., 2001; Xu et al., 2009). This Ca^{2+} must act on the Ca^{2+} sensor which remains in the absence of Syt2.

To characterize the Ca^{2+} sensitivity of spontaneous release in Syt2 KO synapses while avoiding confounding effects of the local Ca^{2+} source, we performed experiments in which 10 mM BAPTA was partially loaded with Ca^{2+} (3 or 7 mM Ca^{2+}; nominal free $[Ca^{2+}]$ of 100 and 500 nM, respectively). This enabled us to increase the free $[Ca^{2+}]_i$ while the remaining free BAPTA should suppress the influence of the local Ca^{2+} source. Using 10 mM BAPTA / 7 mM

Ca^{2+}, the mEPSC frequency was high following presynaptic whole-cell recording (Fig. 4E; 34.1 ± 10.2 Hz, n = 3), a value which was significantly higher than the one observed with 10 mM BAPTA / 0 Ca^{2+} (~ 1.5 Hz, see above; p = 0.029). With 10 mM BAPTA / 3 mM Ca^{2+}, the average mEPSC frequency was 9.1 ± 2.6 Hz (n = 4 cell pairs). These experiments show that the efficiency of BAPTA depends on the amount of loading with Ca^{2+}, and therefore, on the free $[Ca^{2+}]_i$ attained in the nerve terminal, which was independently monitored with fura-2 Ca^{2+} imaging (Fig. 4E, top).

We next investigated whether the spontaneous release in wild-type synapses was also Ca^{2+}-dependent. Syt2 KO synapses rescued with the $Syt2^{WT}$ construct had a low mEPSC frequency before presynaptic whole-cell recording (Fig. 4F; 2.3 ± 1.1 Hz), indicating efficient release clamping by the re-expressed wild-type protein (see also above, Fig. 2). Loading with 10 mM BAPTA / 0 Ca^{2+} did not further reduce the mEPSC frequency (0.82 ± 0.09, n = 5; p = 0.22, paired t-test). Similar results were obtained in Syt2 +/+ synapses, in which BAPTA did not change the mEPSC frequency (p = 0.85; data not shown). Taken together, presynaptic BAPTA strongly suppresses the elevated spontaneous release in Syt2 KO synapses, but leaves spontaneoues release in wild-type synapses largely unaffected, suggesting that in wild-type calyces of Held, spontaneous release is Ca^{2+} independent (see Discussion).

Syt2 clamps a linear Ca^{2+} sensor which can drive spontaneous and asynchronous release

In order to visualize the Ca^{2+} sensitivity of spontaneous release revealed by presynaptic BAPTA loading (see above, Fig. 4), we next plotted the measured mEPSC frequencies obtained under the different Ca^{2+} buffering conditions as a function of $[Ca^{2+}]_i$ (Fig. 5). In this dose-response curve, data under three different molecular conditions are shown: Syt2 KO data (red data points), Syt2 KO data following rescue with $Syt2^{WT}$ (black data points), and Syt2 KO synapses following rescue with the $Syt2^{D3}$ mutant (blue data points). In addition to the

experiments with Ca^{2+} - loaded or free BAPTA illustrated in Fig. 4, the plot also contains data employing weak flashes that produced small $[Ca^{2+}]_i$ steps in the range of ~ 150 nM to ~ 1 µM (Fig. 5; filled triangles, see Lou et al., 2005). The data shows that 10 mM BAPTA in the absence of added Ca^{2+} strongly reduced the elevated mEPSC frequency in Syt2 KO mice, whereas EGTA was nearly inefficient (Fig. 5, red diamond and open round symbol, respectively). Increasing the free $[Ca^{2+}]_i$ in the presence of 10 mM BAPTA led to a near-linear increase of the spontaneous release frequency in the Syt2 KO synapses (Fig. 5; open red squares). The Ca^{2+} uncaging data for higher steps of $[Ca^{2+}]_i$ up to ~ 30 µM are contiguous with the dose-response curve seen in the sub-micromolar range. The Syt2 KO data was fitted with a linear relation in double logarithmic coordinates, yielding a slope of 1.0 (Fig. 5, red line).

In Syt2 KO synapses rescued with the $Syt2^{WT}$ or $Syt2^{D3}$ construct, spontaneous release under 10 mM BAPTA / 0 Ca^{2+} was slightly, but significantly lower than in Syt2 KO synapses (Fig. 5, compare black and red diamond symbols; $p = 0.004$). Importantly, in the range of 10 - ~ 80 nM $[Ca^{2+}]_i$, spontaneous release was not further enhanced by elevating $[Ca^{2+}]_i$, which shows the effect of release clamping present in wild-type Syt2, as well as in the $Syt2^{D3}$ mutant. Synapses rescued with the $Syt2^{WT}$ construct showed a highly supra-linear release above ~ 500 nM (Lou et al., 2005), indicating that Syt2 confers the highly Ca^{2+} cooperative phase of release (Sun et al., 2007). Comparing the $Syt2^{D3}$ mutant data with the Syt2 KO data reveals the effect of release clamping, which leads to a constant, ~ 10 fold reduction of release over a wide range of $[Ca^{2+}]_i$ (Fig. 5; blue and red data points, respectively). Thus, Syt2 suppresses the action of a linear Ca^{2+} sensor by about 10-fold over a large range of $[Ca^{2+}]_i$.

Finally, the availability of the $Syt2^{D3}$ mutant which does not support Ca^{2+}-evoked release, but which shows intact release clamping should allow us to estimate how Syt2 normally clamps

the action of remaining Ca^{2+} sensor(s) in asynchronous release (Fig. 6). In these experiments, we investigated release evoked by AP-like presynaptic depolarizations (100 Hz trains of 1 ms depolarizations to +45 mV), either in Syt2 KO synapses, or in $Syt2^{D3}$ rescue synapses. In Syt2 KO synapses, train stimulation completely lacked synchronous EPSCs of several nanoampere amplitude seen in wild-type synapses (not shown). Instead, there was a substantial build-up of asynchronous release which only slowly decayed after the end of the train (Fig. 6B). Interestingly, in synapses rescued with the $Syt2^{D3}$ mutant, this asynchronous release component was strongly suppressed based on the measured EPSC responses (Fig. 6B, grey trace, and Fig. 6C). Many of the remaining near - quantal release events occurred within 2 ms following the presynaptic Ca^{2+} tail current, and therefore represented remaining synchronous release (Fig. 6B, inset; star symbols). To analyze asynchronous release in the $Syt2^{D3}$ synapses, we counted asynchronously occurring near-quantal EPSCs in a time window of 2 - 10 ms following each presynaptic Ca^{2+}-tail current. This analysis, as well as a comparison of the temporally averaged EPSCs minus the diffuse current calculated by the EPSC deconvolution analysis (Fig. 6C; see Experimental Procedures) both revealed a strong suppression of asynchronous release upon rescue with the $Syt2^{D3}$ mutant (Fig. 6D). . Thus, Syt2 normally strongly suppresses the activity of the remaining Ca^{2+} sensor during trains of presynaptic activity.

Discussion

Here, we established virus - mediated *in-vivo* rescue of presynaptic protein function at the calyx of Held, which has allowed us to perform a structure - function analysis of Syt2 under direct control of presynaptic $[Ca^{2+}]_i$. We separated two main functions of Syt2 in regulating Ca^{2+}-evoked release: the Ca^{2+} triggering of release, and the suppression of other Ca^{2+} sensor(s) that remain in the absence of Syt2 ("release clamping"). We found that mutating an aspartate residue in the Syt2 C_2B domain ($Syt2^{D3}$ mutant) completely abolished Ca^{2+} - evoked

release mediated by Syt2, but importantly, the release clamping function remained intact in the $Syt2^{D3}$ mutant. On the other hand, mutations in the poly-lysine motif of the C_2B domain compromised the release clamping function, whereas Ca^{2+}-evoked release *per se* was fully supported. By making use of the intact release clamping in the $Syt2^{D3}$ mutant, we show that any Ca^{2+} sensor(s) remaining in the absence of Syt2 are normally strongly clamped by Syt2. Together, these data suggest that release clamping by Syt2 suppresses both spontaneous release, as well as evoked asynchronous release mediated by other Ca^{2+} sensors. Thus, our study shows that Syt2, and, in analogy Syt1, enhance the dynamic range of Ca^{2+}-evoked release by acting as a Ca^{2+} sensor for fast transmitter release, as well as by suppressing the activity of remaining Ca^{2+} sensors.

Rescue of Syt2 function at the calyx of Held

We demonstrated that a genetic rescue approach can be successfully applied at the calyx of Held synapse. We used adenovirus-mediated protein expression relying on stereotactic injections into the cochlear nucleus, a method that has been developed and successfully used for overexpression of presynaptic proteins, including Syt2, at the calyx of Held of young rats (Wimmer et al., 2004; Young and Neher, 2009). However, using the rat as a model system has the disadvantage that the endogenous wild-type protein of interest remains at the synapse, limiting the overexpression approach to the study of dominant - negative mutants (Young and Neher, 2009). We therefore established stereotactic surgery in young mice (P6 - P7), and used Syt2 KO mice (Pang et al., 2006a) as a null genetic background for a structure - function analysis of Syt2. We show that 6 - 8 days following stereotactic injection, the recombinant Syt2 protein had been correctly transported to the nerve terminal and was present at a roughly three-fold higher concentration than the wild-type protein in Syt2 +/+ calyces (Fig. 1). Adenovirus-mediated re-expression of Syt2 fully rescued the ~ 500-fold reduction of Ca^{2+} -

evoked release in Syt2 KO mice (Fig. 2), thus allowing for a structure - function analysis of Syt2 at the calyx of Held.

Differential roles of C_2B domain residues in triggering Ca^{2+} - evoked release and in release clamping

In addition to rescuing Ca^{2+}-evoked release, re-expression of $Syt2^{WT}$ also fully reversed the elevated mEPSC frequency seen in Syt2 KO mice (Fig. 2), indicating a genuine release clamping function of Syt2. Release clamping was compromised when the poly-lysine motif of the C_2B domain was neutralized ($Syt2^{3K}$ mutant), although this mutant fully rescued release evoked by Ca^{2+} uncaging (Fig. S2). Biochemical evidence showed that the poly-lysine site binds inositol polyphosphates (Fukuda et al., 1995), and mediates binding of the clathrin adaptor AP2, Ca^{2+} channels (Chapman et al., 1998), and Ca^{2+}-independent SNARE protein binding (Rickman et al., 2004). Previous rescue experiments in hippocampal and Drosophila synapses showed reduced AP-evoked release with poly-lysine site mutants, and a rightward shift in plots of release versus *extracellular* Ca^{2+} concentration (Borden et al., 2005; Li et al., 2006; Loewen et al., 2006). We found that the intrinsic Ca^{2+} sensitivity of release as tested by presynaptic Ca^{2+} uncaging was unchanged, whereas the efficiency of brief Ca^{2+} currents in inducing release was reduced (Fig. S2). These findings strongly suggest that the C_2B poly-lysine site is not involved in setting the intracellular Ca^{2+} sensitivity of release (but see Li et al., 2006). Rather, the effects of the poly-lysine site mutation on release avoked by APs and by brief presynaptic depolarizations could be explained by assuming a role of Syt2 in 'positioning' vesicles close to Ca^{2+} channels, as shown recently using another mutation in the C_2B domain (Young and Neher, 2009).

A mutation of the third aspartate residue in the Ca^{2+} coordination site of the C_2B domain ($Syt2^{D3}$ mutant) fully rescued the clamping of spontaneous release (Fig. 3), and it acted as a

dominant - negative mutant regarding Ca^{2+} - evoked release over a wide range of $[Ca^{2+}]_i$ (Fig. 5). Thus, clamping of spontaneous release, and the suppression of asynchronous release mediated by a remaining Ca^{2+} sensor, likely represents the same clamping function of Synaptotagmins. In principle, release clamping could be explained by two different mechanisms. First, both Syt2 and a second Ca^{2+} sensor could normally be present at the release machinery, and Syt2 would normally suppress the activity of the other Ca^{2+} sensor ("release clamping" model; see Fig. S4A). Alternatively, it has been argued (Groffen et al., 2010) that other Ca^{2+} sensor(s) can access the release machinery only in the absence of Syt1/2 (model of "mutually exclusive presence"; Fig. S4B). One clue lies in our finding that the $Syt2^{3K}$ mutant only weakly supports release clamping despite of its presence at the release machinery, which is evident from the full rescue of Ca^{2+} uncaging - evoked release by this mutant. Thus, we favour a model in which Syt2 and an unknown Ca^{2+} sensor are both present at the release machinery, and where Syt2 normally suppresses the action of the remaining Ca^{2+} sensor. Nevertheless, we do not know the identity of the remaining Ca^{2+} sensor (see Discussion below), and it is therefore difficult to firmly conclude about the molecular mechanism of release clamping.

The Ca^{2+} sensitivity of spontaneous release

We have used direct presynaptic loading of BAPTA and EGTA, as well as partially Ca^{2+} - loaded BAPTA, to clarify the role of presynaptic $[Ca^{2+}]_i$ elevations in the 10's of nanomolar range in modulating spontaneous release. In wild-type synapses, BAPTA did not significantly reduce the mEPSC frequency, showing that neither Ca^{2+} binding to Syt2 at the normal resting $[Ca^{2+}]_i$ (~ 40 - 50 nM; see Fig. S1), nor intracellular Ca^{2+} release events mediate spontaneous release in wild-type calyx of Held synapses. In Syt2 KO calyces, however, the elevated mEPSC frequency of ~ 20 Hz was strongly suppressed by BAPTA, but EGTA was largely inefficient. The selective sensitivity to BAPTA, which is also evident from previous work

using the AM-esters of both buffers (Pang et al., 2006b; Xu et al., 2009), probably indicates that in the absence of Syt2, short-lived Ca^{2+} transients drive spontaneous release events, most likely generated by intracellular Ca^{2+} sources (Fig. S3). Our finding that the basal $[Ca^{2+}]_i$ in the nerve terminal was unchanged in Syt2 KO synapses, together with the sensitivity of spontaneous release to BAPTA, again highlights the fact that local Ca^{2+} transients must be responsible for driving the elevated spontaneous release in Syt2 KO synapses. Although the exact mechanism generating this activity remains unclear at present, it seems important to differentiate between truly spontaneous release at the resting $[Ca^{2+}]_i$ of the nerve terminal, and release driven by intracellular presynaptic Ca^{2+} - release events, the latter of which might imply localized intracellular Ca^{2+} - release transients.

Using partially Ca^{2+} - loaded BAPTA to overcome any local Ca^{2+} sources, we showed that a surprisingly linear Ca^{2+} sensor regulates spontaneous release in Syt2 KO synapses (Figs 4, 5). However, the action of this sensor was strongly suppressed in the $Syt2^{WT}$ rescue synapses and $Syt2^{D3}$ synapses, in which spontaneous release was essentially Ca^{2+} - independent up to ~ 50 - 80 nM $[Ca^{2+}]_i$ (Fig. 5). Therefore, in wild-type synapses, Syt2 strongly suppresses the action of the linear Ca^{2+} sensor, and the remaining spontaneous release is largely Ca^{2+} independent, maybe representing a spontaneous overcoming of the energy barrier of vesicle fusion (Lou et al., 2005; Basu et al., 2007). We observed a slope of 1 - 1.1 of the remaining Ca^{2+} sensor in P12 - P15 Syt2 k.o. mice, whereas Sun et al. (2007) observed a larger slope value (~ 2) in younger mice. This suggests a developmental downregulation of one or several remaining Ca^{2+} sensing proteins, and it indicates that asynchronous release is not generally described by a Ca^{2+} sensor with a cooperativity of 2, as hypothesized by Sun et al. (2007). We conclude that Syt1/2 represent the Ca^{2+} sensors which confer the highly Ca^{2+} cooperative phase of release above ~ 0.5 µM $[Ca^{2+}]_i$, but that additional Ca^{2+} sensors are likely present as well. Molecularly realistic models of Ca^{2+} -triggering of release would therefore have to assume the

presence of several Ca^{2+} sensors (Sun et al., 2007), but in addition, the mechanisms of release clamping of further Ca^{2+} sensors by Syt1/2 need to be included, and the Ca^{2+} cooperativity of the remaining sensor(s) should be assessed.

The molecular nature and physiological role of the remaining Ca^{2+} sensor

The identity of the near-linear Ca^{2+} sensor which remains in the absence of Syt2 is currently unknown (see also Discussion in Sun et al., 2007). There are about 15 currently known Syt isoforms in mammals, and of these, Syt1, -2, -3, -5, -6, -7, -9, and Syt10 bind Ca^{2+} (Pang and Südhof, 2010). Amongst these isoforms, a recent single-cell qPCR study in putative calyx of Held - generating bushy cells has shown the expression of Syt3, Syt5 (in young neurons only), and Syt7, besides Syt2 (Xiao et al., 2010). A quite similar expression profile for the non - Syt1/2 isoforms was found in hippocampal basket cell interneurons (Kerr et al., 2008). Interestingly, removal of Syt7 at the zebrafish NMJ selectively reduced the slow release component, making Syt7 a candidate Ca^{2+} sensor for slow release (Wen et al., 2010). Syt7, in conjunction with Syt1, is also a Ca^{2+} sensor for release in chromaffin cells (Schonn et al., 2008), but Syt7 KO did not affect release in cortical inhibitory synapses (Maximov et al., 2008). Beyond Syts, it has recently been proposed that Doc2B represents the Ca^{2+} sensor for spontaneous release in hippocampal neurons (Groffen et al., 2010), but it is uncertain whether Doc2B can drive release over ~ 3 orders of magnitude as observed here for the Ca^{2+} sensor remaining in the absence of Syt2 (Fig. 5). Taken together, more work is needed to identify the Ca^{2+} sensors that remain in Syt1/2 KO synapses.

What is the possible physiological role of the remaining Ca^{2+} sensor in asynchronous release? Although it is often assumed that a separate Ca^{2+} sensor mediates asynchronous release (Goda and Stevens, 1994; Otsu et al., 2004; Sun et al., 2007), we showed that the action of the 'remaining' Ca^{2+} sensor in asynchronous release is normally strongly suppressed by Syt2 (Fig.

6). Asynchronous release at the wild-type calyx of Held following 100 Hz trains is low, as shown by EPSC fluctuation analysis (Scheuss et al., 2007); thus, the calyx of Held has a high ratio of fast versus asynchronous release. This is of physiological relevance for these auditory neurons which signal with fast membrane potential changes (Trussell, 1999), enabling them to follow high rates of AP firing (Futai et al., 2001; Taschenberger et al., 2002). Therefore, the release clamping function of Syt2 demonstrated here is physiologically relevant in suppressing the activity of more slowly transducing Ca^{2+} sensor(s) for transmitter release during trains of high-frequency activity.

Experimental Procedures

DNA cloning

The wild-type Syt2 rescue construct ($Syt2^{WT}$) was produced from the rat Syt2 cDNA (NM_012665) by addition of a sequence encoding for the myc epitope (MASEQKLISEEDLGS) directly upstream of the Syt2 ORF, tagging the Syt2 protein at the intravesicular N-terminus. The C_2B domain deletion mutant ($Syt2^{\Delta C2B}$) was obtained by insertion of a stop codon after the residue G266. A single aspartate to asparagine mutation (D364N; called $Syt2^{D3}$ mutant), a triple lysine to glutamine mutation (K327Q, K328Q, K332Q; called $Syt2^{3K}$), and the combination of both mutants (K327Q, K328Q, K332Q, D364N; called $Syt2^{3K/D3}$) were obtained using PCR-based mutagenesis (see Suppl. Exp. Procedures for the primers used). All the DNA constructs were verified by sequencing.

Adenovirus vector

We used a modified 2nd generation E1-, E2a-, and E3- deleted serotype 5 adenovirus system (Zhou and Beaudet, 2000), kindly provided by Dr. Sam Young. The adenovirus system used here did not include the further enhancements referred to as 'pUNISHER' by Young and Neher (2009). Ad: hSyn-Syt2: hSyn-eGFP viruses were prepared by placing a Syt2 expression cassette (containing either $Syt2^{WT}$, $Syt2^{\Delta C2B}$, $Syt2^{D3}$, $Syt2^{3K}$, or $Syt2^{3K/D3}$; see above) under the control of the hSyn promoter in the shuttle vector, combined with a modified backbone vector containing an eGFP expression cassette with a second hSyn promotor in the E2a locus of the adenoviral genome. For the expression of eGFP alone (ad: hSyn-eGFP virus), a 'dark' backbone without eGFP insert was used, and the hSyn-eGFP expression cassette was placed in the shuttle vector. For virus preparation, see Suppl. Experimental Procedures.

Transgenic mice and surgery

All procedures of mouse breeding, handling and surgery were approved by the Veterinary office of the Canton of Vaud, Switzerland (authorizations 1880, 2063). We performed heterozygous breeding of Syt2 -/- mice (Pang et al., 2006b). P6 - P7 pups (3 - 4 g weight) were unilaterally injected under isoflurane anaesthesia (Minrad Inc., Buffalo, NY, USA) with adenovirus into the VCN using, in general, the stereotactic injection protocols developed by Wimmer et al. (2004) for rats. Adenovirus (0.2 μl/site) was injected at a rate of 0.08 μl/min using a 10 μl Hamilton syringe (Hamilton, Bonaduz, Switzerland) and SP100i syringe pump (WPI, Aston, UK) in a total of six sites (two 0.2 mm vertically-spaced sites at each of three 0.25 mm rostra-caudally spaced positions; see Suppl. Exp. Procedures for details). After the injections, the skin was closed using Histoacryl glue (B. Braun, Melsungen, Germany), and the animal was returned to the mother after ~0.5 - 1 hour of recovery. Animals were used for experiments at the age P12 - P15, corresponding to 6 - 8 days post-injection.

Immunohistochemistry

Animals were transcardially perfused with 4% paraformaldehyde in phosphate-buffered saline. Free-floating 30 μm brainstem slices containing the medial nucleus of the trapezoid body (MNTB) were immunostained for Syt2 and eGFP (Fig. 1) by standard protocols as described before (Xiao et al., 2010), using primary mouse monoclonal anti-Syt2 (‘znp-1’, ZIRC, Univ. of Oregon, Eugene, OR, USA, see Fox and Sanes, 2007), rabbit polyclonal anti-VGluT2 (135403, Synaptic Systems, Göttingen, Germany) and chicken polyclonal anti-GFP (Ab13970, Abcam, Cambridge, UK) antibodies (see Suppl. Exp. Procedures for the secondary antibodies, staining protocol and confocal imaging). The antibodies were tested for cross-reactivity, and anti-Syt2 antibody showed no signal in slices from Syt2 KO mice (see also Fig. 1). Quantitative image analysis (Fig. 1C-F) was performed with custom routines in IgorPro (WaveMetrics, Lake Oswego, OR, USA). In brief, regions of interest (ROI) were drawn by

hand around each calyx of Held. Low-pass filtered VGluT2 images of each calyx were individually thresholded to generate analysis masks within drawn ROIs. The resulting masks were used to sample the local background-corrected fluorescence from VGluT2, eGFP and Syt2 channels.

Slice preparation and electrophysiology

Transverse 180 - 200 µm slices at the level of MNTB were obtained using a Leica VT 1000S slicer (Leica Microsystems) and kept at 37°C in a bicarbonate-buffered solution (see Suppl. Exp. Procedures). The extracellular solutions were bicarbonate-buffered solutions, which, for paired recordings, contained tetraethylammonium chloride (TEA, 10 mM), tetrodotoxin (TTX, 1 µM), D-2-Amino-5-phosphonopentanoic acid (D-AP5, 50 µM), γ-D-glutamylglycine (γ-DGG, 2 mM), cyclothiazide (CTZ, 100 µM), bicuculline (10 µM) and strychnine (2 µM). In experiments where only mEPSCs were recorded (Figs. 4, S3), γ-DGG was omitted. Whole-cell recordings from pre- and postsynaptic compartments (see Suppl. Exp. Procedures for detailed pipette solutions) were made at room temperature (21 - 25°C) using an EPC-10/2 double patch-clamp amplifier (HEKA Elektronik, Lambrecht/Pfalz, Germany) under control of PatchMaster software (HEKA).

Ca^{2+} uncaging and Ca^{2+} imaging

Ca^{2+} uncaging experiments were done similarly as described (Lou et al., 2005; Wölfel et al., 2007; Kochubey et al., 2009). The presynaptic intracellular solution (see Suppl. Exp. Procedures) was supplemented with 0.1 mM fura-2FF (TefLabs, Austin, TX, USA), 2 or 5 mM DM-Nitrophen (Merck-Calbiochem) and 1.75 or 4.52 mM $CaCl_2$, for flashes aiming at $[Ca^{2+}]_i$ steps below, or above 20 µM, respectively. For loading 10 mM BAPTA/0 Ca^{2+} or 10 mM EGTA into calyces (Fig. 4A, C, F), the presynaptic solution was supplemented with (in mM) 0.1 fura-2 and 10 Cs-BAPTA or 10 Cs-EGTA, pH 7.2. To partially load 10 mM BAPTA

with Ca^{2+} (Fig. 4E), 3.14 or 7.02 mM $CaCl_2$ were added for predicted free [Ca^{2+}] of 100 or 500 nM, respectively. The elevated mEPSC frequency in experiments with elevated $[Ca^{2+}]_i$ should not lead to a depletion of the readily-releasable pool, since the rates of pool recovery below ~ 1 µM $[Ca^{2+}]_i$ are several fold higher than the release rates (Neher and Sakaba, 2008). Some of the data in these experiments were obtained after retraction of the presynaptic pipette, followed by a gradual decrease in $[Ca^{2+}]_i$ as measured by fura-2, which enabled further modulation of presynaptic $[Ca^{2+}]_i$ in the presence of BAPTA (Fig. 5, open squares).

Data analysis

The transmitter release rates were estimated by EPSC deconvolution, using the deconvolution procedure introduced by Neher and Sakaba (2001). The deconvolution analysis assumed that individual mEPSCs summed linearly and decayed with double-exponential kinetics (Schneggenburger and Neher, 2000). Release rates were corrected for the predicted 'spill-over' current, with simulation parameters estimated using “template protocols” as described in Neher and Sakaba (2001). However, for Syt2 KO synapses, as well as in $Syt2^{D3}$ and $Syt2^{3K/D3}$ rescue experiments, the use of template protocols was not possible because of the absence of phasic EPSCs in template protocols. In these cases, the parameters for simulating the spill-over current were fixed to values similar to those observed in $Syt2^{WT}$ synapses. The mEPSC parameters used in the deconvolution analysis were determined from average mEPSC waveforms obtained in each cell. mEPSCs were detected by an analysis routine in IgorPro, implementing template-matching detection algorithm (Clements and Bekkers, 1997). Statistical significance, unless specified, was assessed by unpaired two-sample t-test; significance levels were indicated by asterisks using the convention: * $p < 0.05$, ** $p < 0.01$, *** $p < 0.001$.

Acknowledgements

We thank Dr. Sam Young for advice on virus vectors and for providing the modified adenovirus genomic and shuttle DNA plasmids, Drs. R. Adachi and Tomas Südhof for providing the Syt2 KO mice, Drs. H. Zhou and A. Beaudet for allowing us to use the E2T packaging cell line, Heather Murray for excellent technical assistance and Dr. David Perkel for critical reading of the manuscript. This study was supported by the Swiss National Science Foundation (Grant # 3100A0_122496/1).

Figure Legends

Figure 1. Correct targeting of recombinant Syt2 to nerve terminals, and quantification of Syt2 overexpression.

(A) Immunostaining with antibodies against eGFP (green) and Syt2 (red) on a transverse section through the MNTB area of a P13 Syt2 KO mouse. The mouse was stereotactically injected at P6 with an adenovirus driving the expression of wild-type Syt2 ($Syt2^{WT}$), and eGFP. Note numerous eGFP - positive fibers crossing the midline into the MNTB contralateral to the injected VCN. The ipsilateral MNTB is devoid of eGFP labelled terminals except one (arrowhead). Note the absence of Syt2 immunohistochemical signal in the ipsilateral MNTB of this Syt2 KO mouse, which confirms the specificity of the anti Syt2 antibody (znp-1 antibody; see Experimental Procedures).

(B) Images at higher magnification (white rectangle in B) show that the Syt2 signal was localized specifically in the nerve terminal region of eGFP - positive calyces (arrowheads), whereas the diffusible eGFP was present in both the synaptic terminals and adjacent axonal compartments (arrows).

(C, D) Triple immunolabeling against eGFP (green), vesicular glutamate transporter 2 (VGluT2, blue) and Syt2 (red) is shown for a P13 Syt2 KO mouse expressing $Syt2^{WT}$ (C), and of a littermate sham-injected Syt2 +/+ mouse (D). Identical staining and imaging parameters (see Experimental Procedures) resulted in VGluT2 labelling of the calyx terminals with similar intensity in both cases, while Syt2 immunofluorescence appeared brighter in eGFP-positive KO synapses, than in the Syt2 +/+ mouse. Arrowhead in (C) indicates a single non-infected (eGFP-negative) calyx of Held, which was also devoid of Syt2 signal.

(E, F) Quantification of VGluT2 (E) and of Syt2 (F) immunofluorescence at three types of calyces: first, eGFP-positive calyces in the Syt2 KO mouse (thus, $Syt2^{WT}$-expressing calyces; red bars; n = 218); second, eGFP-negative calyces in the same Syt2 KO mouse (pink bars; n =

128); third, calyces of Held in the sham-injected Syt2 +/+ mouse (open black bars; n = 177). Note the similar level of VGluT2 expression amongst all three types of calyces, but ~3 fold higher level of Syt2 immunofluorescence in Syt2 KO calyces expressing recombinant $Syt2^{WT}$, as compared to calyces in Syt2 wild-type mice.

Error bars = SD.

Figure 2. Rescue of Ca^{2+}-evoked release and of the clamping of spontaneous release by *in-vivo* $Syt2^{WT}$ expression

(A1-C1) Example Ca^{2+} - uncaging experiments in eGFP-expressing calyces of Held from a Syt2 +/+ mouse (A1), a Syt2 KO mouse (B1), and from a Syt2 KO mouse following expression of $Syt2^{WT}$ + eGFP (C1). The presynaptic eGFP signal is shown by fluorescent images of the calyces (insets; scale bars 10 μm). $[Ca^{2+}]_i$ steps elicited by Ca^{2+} - uncaging (*top*), EPSCs (*middle*) and transmitter release rates (*bottom*) are shown. Note the different y-scales that apply to the black and grey traces (*middle* and *bottom*). The large and fast EPSC (C1) demonstrates full rescue of Ca^{2+}-evoked release by expression of $Syt2^{WT}$.

(A2-C2) mEPSC recordings obtained in the same cells as shown in (A1-C1). Note the elevated mEPSC frequency recorded in the Syt2 KO calyx (B2), and the low mEPSC frequency apparent after re-expression of $Syt2^{WT}$ (C2).

(D) Average peak release rates for $[Ca^{2+}]_i$ steps in the range of 7 - 20 μM, analyzed for eGFP expressing wild-type synapses (grey bar; see A1), for eGFP expressing Syt2 KO synapses (red bar; see B1), and for Syt2 KO synapses in which $Syt2^{WT}$ was expressed (black bar; see C1). Note the full rescue of Ca^{2+}-evoked release following Syt2 expression.

(E) Average mEPSC frequency for the same three conditions as shown in (D). Note that $Syt2^{WT}$ rescue (black bar, *right*) completely re-established spontaneous release clamping.

(F, G) $[Ca^{2+}]_i$ - dependence of the peak release rate (F) and of the synaptic delay (G) in $Syt2^{WT}$ rescue (black) and control synapses (grey), shown on a double-logarithmic scale. The data was fitted by an allosteric model for Ca^{2+} binding and vesicle fusion (black line, see Suppl. Experimental Procedures). The release rates obtained in Syt2 KO synapses (red) were fitted by a line in double - logarithmic scales, yielding a slope of 1.1 (red line).

Error bars = SEM. See also Fig. S1.

Figure 3. Separate residues in the Syt2 C_2B domain trigger Ca^{2+}-evoked release and mediate spontaneous release clamping.

(A - D) Representative Ca^{2+}-uncaging experiments in Syt2 KO synapses rescued with different Syt2 mutant constructs as indicated. Presynaptic $[Ca^{2+}]_i$ steps elicited by Ca^{2+} -uncaging (*top*), EPSCs (*middle*) and transmitter release rates (*bottom*) are shown. Panels (A2 - D2) show spontaneous mEPSC recordings from the corresponding cells. The inset in C1 shows the Ca^{2+}-evoked EPSC and the transmitter release rate at a higher time resolution for the $Syt2^{3K}$ mutant. Note the differential rescue of Ca^{2+}-evoked release and release clamping by the $Syt2^{D3}$ and $Syt2^{3K}$ mutants.

(E) Average peak release rates analyzed for $[Ca^{2+}]_i$ steps of 7 - 20 μM amplitude, for the different rescue constructs shown in (A - D), and for the Syt2 KO synapses and $Syt2^{WT}$ rescue synapses (Fig. 2). Note the complete rescue of Ca^{2+}-evoked release by the $Syt2^{3K}$ mutant.

(F) Average mEPSC frequency for the different rescue constructs. Note the differential suppression of the elevated mEPSC frequency by the $Syt2^{D3}$ and $Syt2^{3K}$ mutant.

(G) Scheme of the Syt2 mutant constructs used here.

Error bars = SEM. See also Fig. S2.

Figure 4. The intracellular Ca^{2+} - sensitivity of spontaneous release in Syt2 KO calyces.

(A) Example of a recording in which a calyx of Held from a Syt2 KO mouse was loaded with 10 mM BAPTA / 0 Ca^{2+} through the presynaptic patch pipette. Top panel, presynaptic $[Ca^{2+}]_i$ measured by fura-2 Ca^{2+} imaging; bottom panel, average mEPSC frequency measured over 5s intervals. Arrowhead marks the time when the whole-cell patch-clamp configuration was achieved. Note the rapid decrease in mEPSC frequency after establishing the presynaptic whole-cell recording. The insets show example traces of mEPSCs at the times indicted in the bottom panel.

(B) Average mEPSC frequency before and after presynaptic loading with 10 mM BAPTA / 0 Ca^{2+} for n = 4 cells.

(C) Example of an experiment in which a Syt2 KO calyx was loaded with 10 mM EGTA / 0 Ca^{2+} . Note that in contrast to BAPTA (A), the mEPSC frequency was only gradually reduced by ~ 20%.

(D) Average mEPSC frequency before and after presynaptic loading with 10 mM EGTA / 0 Ca^{2+} for n=8 cells. Note the differential effect of the fast and slow Ca^{2+} buffers on the mEPSC frequency in Syt2 KO synapses.

(E) Similar experiment as in (A), but 10 mM BAPTA in the presynaptic patch pipette was partially loaded with 7 mM $CaCl_2$ (predicted free $[Ca^{2+}]_i$ = 500 nM). Note the high mEPSC frequency maintained in the Syt2 KO synapse after achieving the presynaptic whole-cell recording.

(F) Loading 10 mM BAPTA / 0 Ca^{2+} into a wild-type calyx of Held did not change the spontaneous mEPSC frequency.

Error bars = SEM. See also Fig. S3.

Figure 5. Syt2 normally clamps a near-linear remaining Ca^{2+} sensor over a wide range of $[Ca^{2+}]_i$.

Summarized $[Ca^{2+}]_i$ - dependence of spontaneous and flash-evoked release in the Syt2 KO synapses (red symbols), in Syt2 KO synapses rescued with the $Syt2^{WT}$ construct (black symbols), and in Syt2 KO synapses rescued with the $Syt2^{D3}$ construct (blue symbols). Data from the experiments of the $[Ca^{2+}]_i$ -sensitivity of spontaneous release using presynaptic BAPTA loading (diamond symbols, and squares) are shown. In addition, data from weak flashes (triangles), and from strong flashes (circles; see Figures 2, 3) are summarized here. Note that the data with $Syt2^{D3}$ rescue, in which the release clamping function is intact, shows an ~ 10 - fold lower release rate as compared to the Syt2 KO data over a large range of $[Ca^{2+}]_i$. Below 100 nM $[Ca^{2+}]_i$, spontaneous release in $Syt2^{WT}$ or $Syt2^{D3}$ synapses was low, and had a shallow Ca^{2+}-dependency. The data of the Syt2 KO synapses was fitted by linear regression in double-logarithmic coordinates, revealing a slope of 1.0 (red line; fit range 20 nM - 70 µM). The data of the $Syt2^{D3}$ synapses was similarly fitted by a line, giving a slope of 1.0 (fit range, 100 nM - 20 µM $[Ca^{2+}]_i$). The $Syt2^{WT}$ data was fitted with the allosteric model of Ca^{2+} binding and vesicle fusion (see Suppl. Experimental Procedures for fit parameters).

Figure 6. Syt2 strongly clamps asynchronous release during trains of AP-like stimuli as demonstrated by rescue with the $Syt2^{D3}$ mutant.

(A - B) Representative experiments from a Syt2 KO calyx of Held (black traces) and from a Syt2 KO calyx rescued with the $Syt2^{D3}$ construct (grey traces), stimulated with a train of presynaptic AP -like depolarizations (from -80 to +45 mV for 1 ms, 100 Hz). (A), presynaptic Ca^{2+} currents and (B) EPSCs in response to trains of AP - like depolarizations. The bottom panel of (B) shows the transmitter release rate from the Syt2 KO synapse; the fine black trace in (B) is the glutamate spill-over current estimated during the EPSC deconvolution analysis

(see Experimental Procedures; Neher and Sakaba, 2001). The inset in (B) shows Ca^{2+} currents and EPSC traces during the time indicated by the black line in B on a higher time scale. Note the strongly suppressed asynchronous release following rescue with the $Syt2^{D3}$ mutant. In addition, most of the near-quantal release events remaining in the $Syt2^{D3}$ rescue are synchronous release events occurring within 2 ms of the presynaptic Ca^{2+} current (see star symbols in the inset).

(C) Average value of the temporally averaged EPCS minus the estimated spill-over current, attained during the 20^{th} stimulation, analyzed as a rough measure of asynchronous release. Note that the amount of asynchronous release was strongly reduced by rescue with the $Syt2^{D3}$ mutant, to ~ 9 % of the level observed in the Syt2 KO synapses.

(D) Comparison of the transmitter release rates for the Syt2 KO synapses (open bar), and the $Syt2^{D3}$ synapses (grey bar). Because of the strongly different EPSC amplitudes, deconvolution was used for the estimate of the Syt2 KO synapses, whereas asynchronously occurring mEPSCs were counted for the $Syt2^{D3}$ synapse. The release rate in the $Syt2^{D3}$ rescue synapses was only 1.3% of that in the Syt2 KO synapses.

Error bars = SEM.

References

Adler, E. M., Augustine, G. J., Duffy, S. N., and Charlton, M. P. (1991). Alien intracellular calcium chelators attenuate neurotransmitter release at the squid giant synapse. J Neurosci *11*, 1496-1507.

Basu, J., Betz, A., Brose, N., and Rosenmund, C. (2007). Munc-13-1 C1 domain activation lowers the energy barrier for synaptic vesicle fusion. J Neuroscience *27*, 1200-1210.

Bollmann, J. H., Sakmann, B., and Borst, J. G. (2000). Calcium sensitivity of glutamate release in a calyx-type terminal. Science *289*, 953-957.

Borden, C. R., Stevens, C. F., Sullivan, J. M., and Zhu, Y. (2005). Synaptotagmin mutants Y311N and K326/327A alter the calcium dependence of neurotransmission. Mol Cell Neurosci *29*, 462-470.

Cant, N. B., and Benson, C. G. (2003). Parallel auditory pathways: projection patterns of the different neuronal populations in the dorsal and ventral cochlear nuclei. Brain Res Bull *60*, 457-474.

Chapman, E. R., Desai, R. C., Davis, A. F., and Tornehl, C. K. (1998). Delineation of the oligomerization, AP-2 binding, and synprint binding region of the C2B domain of synaptotagmin. J Biol Chem *273*, 32966-32972.

Chen, Y. A., and Scheller, R. H. (2001). SNARE-mediated membrane fusion. Nat Rev Mol Cell Biology *2*, 98-106.

Chicka, M. C., Hui, E., Liu, H., and Chapman, E. R. (2008). Synaptotagmin arrests the SNARE complex before triggering fast, efficient membrane fusion in response to Ca^{2+}. Nat Struct Mol Biol *15*, 827-835.

Clements, J. D., and Bekkers, J. M. (1997). Detection of spontaneous synaptic events with an optimally scaled template. Biophysical J *73*, 220-229.

Desai, R. C., Vyas, B., Earles, C. A., Littleton, J. T., Kowalchyck, J. A., Martin, T. F., and Chapman, E. R. (2000). The C2B domain of synaptotagmin is a Ca^{2+}-sensing module essential for exocytosis. J Cell Biol *150*, 1125-1136.

Dodge, F. A., Jr., and Rahamimoff, R. (1967). Co-operative action a calcium ions in transmitter release at the neuromuscular junction. J Physiol *193*, 419-432.

Emptage, N. J., Reid, C. A., and Fine, A. (2001). Calcium stores in hippocampal synaptic boutons mediate short-term plasticity, store-operated Ca^{2+} entry, and spontaneous transmitter release. Neuron *29*, 197-208.

Fox, M. A., and Sanes, J. R. (2007). Synaptotagmin I and II are present in distinct subsets of central synapses. J Comp Neurol *503*, 280-296.

Fukuda, M., Kojima, T., Aruga, J., Niinobe, M., and Mikoshiba, K. (1995). Functional diversity of C2 domains of synaptotagmin family. Mutational analysis of inositol high polyphosphate binding domain. J Biol Chem *270*, 26523-26527.

Futai, K., Okada, M., Matsuyama, K., and Takahashi, T. (2001). High-fidelity transmission acquired via a developmental decrease in NMDA receptor expression at an auditory synapse. J Neuroscience *21*, 3342-3349.

Geppert, M., Archer, B. T., III, and Südhof, T. C. (1991). Synaptotagmin II. A novel differentially distributed form of synaptotagmin. J Biol Chem *266*, 13548-13552.

Geppert, M., Goda, Y., Hammer, R. E., Li, C., Rosahl, T. W., Stevens, C. F., and Südhof, T. C. (1994). Synaptotagmin I: A major Ca^{2+} sensor for transmitter release at a central synapse. Cell *79*, 717-727.

Goda, Y., and Stevens, C. F. (1994). Two components of transmitter release at a central synapse. Proc Natl Acad Sci USA *91*, 12942-12946.

Groffen, A. J., Martens, S., Arazola, R. D., Cornelisse, L. N., Lozovaya, N., de Jong, A. P., Goriounova, N. A., Habets, R. L., Takai, Y., Borst, J. G., *et al.* (2010). Doc2b Is a high-affinity Ca^{2+} sensor for spontaneous neurotransmitter release. Science *327*, 1614-1618.

Jahn, R., Lang, T., and Südhof, T. C. (2003). Membrane fusion. Cell *112*, 519-533.

Kerr, A. M., Reisinger, E., and Jonas, P. (2008). Differential dependence of phasic transmitter release on synaptotagmin 1 at GABAergic and glutamatergic hippocampal synapses. Proc Natl Acad Sci U S A *105*, 15581-15586.

Kochubey, O., Han, Y., and Schneggenburger, R. (2009). Developmental regulation of the intracellular Ca^{2+} sensitivity of vesicle fusion and Ca^{2+}-secretion coupling at the rat calyx of Held. J Physiol *587*, 3009-3023.

Kügler, S., Kilic, E., and Bähr, M. (2003). Human synapsin 1 gene promoter confers highly neuron-specific long-term transgene expression from an adenoviral vector in the adult rat brain depending on the transduced area. Gene Ther *10*, 337-347.

Li, L., Shin, O. H., Rhee, J. S., Arac, D., Rah, J. C., Rizo, J., Südhof, T., and Rosenmund, C. (2006). Phosphatidylinositol phosphates as co-activators of Ca^{2+} binding to C_2 domains of synaptotagmin 1. J Biol Chem *281*, 15845-15852.

Littleton, J. T., Stern, M., Perin, M., and Bellen, H. J. (1994). Calcium dependence of neurotransmitter release and rate of spontaneous vesicle fusions are altered in Drosophila synaptotagmin mutants. Proc Natl Acad Sci U S A *91*, 10888-10892.

Liu, H., Dean, C., Arthur, C. P., Dong, M., and Chapman, E. R. (2009). Autapses and networks of hippocampal neurons exhibit distinct synaptic transmission phenotypes in the absence of synaptotagmin I. J Neurosci *29*, 7395-7403.

Llano, I., Gonzalez, J., Caputo, C., Lai, F. A., Blayney, L. M., Tan, Y. P., and Marty, A. (2000). Presynaptic calcium stores underlie large-amplitude miniature IPSCs and spontaneous calcium transients. Nat Neurosci *3*, 1256-1265.

Loewen, C. A., Lee, S. M., Shin, Y. K., and Reist, N. E. (2006). C2B polylysine motif of synaptotagmin facilitates a Ca^{2+}-independent stage of synaptic vesicle priming in vivo. Mol Biol Cell *17*, 5211-5226.

Lou, X., Scheuss, V., and Schneggenburger, R. (2005). Allosteric modulation of the presynaptic Ca^{2+} sensor for vesicle fusion. Nature *435*, 497-501.

Mackler, J. M., Drummond, J. A., Loewen, C. A., Robinson, I. M., and Reist, N. E. (2002). The C_2B Ca^{2+} -binding motif of synaptotagmin is required for synaptic transmission *in vivo*. Nature *418*, 340-344.

Mackler, J. M., and Reist, N. E. (2001). Mutations in the second C2 domain of synaptotagmin disrupt synaptic transmission at Drosophila neuromuscular junctions. J Comp Neurol *436*, 4-16.

Marqueze, B., Boudier, J. A., Mizuta, M., Inagaki, N., Seino, S., and Seagar, M. (1995). Cellular localization of synaptotagmin I, II, and III mRNAs in the central nervous system and pituitary and adrenal glands of the rat. J Neuroscience *15*, 4906-4917.

Maximov, A., Lao, Y., Li, H., Chen, X., Rizo, J., Sorensen, J. B., and Sudhof, T. C. (2008). Genetic analysis of synaptotagmin-7 function in synaptic vesicle exocytosis. Proc Natl Acad Sci U S A *105*, 3986-3991.

Maximov, A., and Südhof, T. C. (2005). Autonomous function of synaptotagmin 1 in triggering synchronous release independent of asynchronous release. Neuron *48*, 547-554.

Neher, E. (1998). Vesicle pools and Ca^{2+} microdomains: new tools for understanding their roles in neurotransmitter release. Neuron *20*, 389-399.

Neher, E., and Sakaba, T. (2001). Combining deconvolution and noise analysis for the estimation of transmitter release rates at the calyx of Held. J Neuroscience *21*, 444-461.

Neher, E., and Sakaba, T. (2008). Multiple roles of calcium ions in the regulation of neurotransmitter release. Neuron *59*, 861-872.

Nishiki, T., and Augustine, G. J. (2004). Dual roles of the C_2B domain of synaptotagmin I in synchronizing Ca^{2+}-dependent neurotransmitter release. J Neurosci *24*, 8542-8550.

Otsu, Y., Shahrezaei, V., Li, B., Raymond, L. A., Delaney, K. R., and Murphy, T. H. (2004). Competition between phasic and asynchronous release for recovered synaptic vesicles at developing hippocampal autaptic synapses. J Neuroscience *24*, 420-433.

Pang, Z. P., Melicoff, E., Padgett, D., Liu, Y., Teich, A. F., Dickey, B. F., Lin, W., Adachi, R., and Südhof, T. C. (2006a). Synaptotagmin-2 is essential for survival and contributes to Ca^{2+} triggering of neurotransmitter release in central and neuromuscular synapses. J Neurosci *26*, 13493-13504.

Pang, Z. P., and Südhof, T. C. (2010). Cell biology of Ca^{2+}-triggered exocytosis. Curr Opin Cell Biol *22*, 496-505.

Pang, Z. P., Sun, J., Rizo, J., Maximov, A., and Südhof, T. C. (2006b). Genetic analysis of synaptotagmin 2 in spontaneous and Ca^{2+}-triggered neurotransmitter release. EMBO J *25*, 2039-2050.

Rickman, C., Archer, D. A., Meunier, F. A., Craxton, M., Fukuda, M., Burgoyne, R. D., and Davletov, B. (2004). Synaptotagmin interaction with the syntaxin/SNAP-25 dimer is mediated by an evolutionarily conserved motif and is sensitive to inositol hexakisphosphate. J Biol Chem *279*, 12574-12579.

Rickman, C., Jimenez, J. L., Graham, M. E., Archer, D. A., Soloviev, M., Burgoyne, R. D., and Davletov, B. (2006). Conserved prefusion protein assembly in regulated exocytosis. Mol Biol Cell *17*, 283-294.

Robinson, I. M., Ranjan, R., and Schwarz, T. L. (2002). Synaptotagmins I and IV promote transmitter release independently of Ca^{2+} binding in the C_2A domain. Nature *418*, 336-340.

Scheuss, V., Taschenberger, H., and Neher, E. (2007). Kinetics of both synchronous and asynchronous quantal release during trains of action potential-evoked EPSCs at the rat calyx of Held. J Physiol *585*, 361-381.

Schneggenburger, R., and Neher, E. (2000). Intracellular calcium dependence of transmitter release rates at a fast central synapse. Nature *406*, 889-893.

Schonn, J. S., Maximov, A., Lao, Y., Sudhof, T. C., and Sorensen, J. B. (2008). Synaptotagmin-1 and -7 are functionally overlapping Ca^{2+} sensors for exocytosis in adrenal chromaffin cells. Proc Natl Acad Sci U S A *105*, 3998-4003.

Stevens, C. F., and Sullivan, J. M. (2003). The synaptotagmin C2A domain is part of the calcium sensor controlling fast synaptic transmission. Neuron *39*, 299-308.

Sun, J., Pang, Z. P., Qin, D., Fahim, A. T., Adachi, R., and Südhof, T. C. (2007). A dual-Ca^{2+}-sensor model for neurotransmitter release in a central synapse. Nature *450*, 676-682.

Taschenberger, H., Leao, R. M., Rowland, K. C., Spirou, G. A., and v. Gersdorff, H. (2002). Optimizing synaptic architecture and efficiency for high-frequency transmission. Neuron *36*, 1127-1143.

Trussell, L. O. (1999). Synaptic mechanisms for coding timing in auditory neurons. Annu Rev Physiol *61*, 477-496.

Wang, L. Y., Neher, E., and Taschenberger, H. (2008). Synaptic vesicles in mature calyx of Held synapses sense higher nanodomain calcium concentrations during action potential-evoked glutamate release. J Neurosci *28*, 14450-14458.

Wen, H., Linhoff, M. W., McGinley, M. J., Li, G. L., Corson, G. M., Mandel, G., and Brehm, P. (2010). Distinct roles for two synaptotagmin isoforms in synchronous and asynchronous transmitter release at zebrafish neuromuscular junction. Proc Natl Acad Sci U S A *107*, 13906-13911.

Wimmer, V. C., Nevian, T., and Kuner, T. (2004). Targeted in vivo expression of proteins in the calyx of Held. Pflugers Arch *449*, 319-333.

Wölfel, M., Lou, X., and Schneggenburger, R. (2007). A mechanism intrinsic to the vesicle fusion machinery determines fast and slow transmitter release at a large CNS synapse. J Neurosci *27*, 3198-3210.

Xiao, L., Han, Y., Runne, H., Murray, H., Kochubey, O., Luthi-Carter, R., and Schneggenburger, R. (2010). Developmental expression of Synaptotagmin isoforms in single calyx of Held-generating neurons. Mol Cell Neurosci *44*, 374-385.

Xu, J., Pang, Z. P., Shin, O. H., and Südhof, T. C. (2009). Synaptotagmin-1 functions as a Ca^{2+} sensor for spontaneous release. Nat Neurosci *12*, 759-766.

Yoshihara, M., Adolfsen, B., and Littleton, J. T. (2003). Is synaptotagmin the calcium sensor? Curr Opin Neurobiol *13*, 315-323.

Yoshihara, M., and Littleton, J. T. (2002). Synaptotagmin I functions as a calcium sensor to synchronize neurotransmitter release. Neuron *36*, 897-908.

Young, S. M., Jr., and Neher, E. (2009). Synaptotagmin has an essential function in synaptic vesicle positioning for synchronous release in addition to its role as a calcium sensor. Neuron *63*, 482-496.

Zhou, H., and Beaudet, A. L. (2000). A new vector system with inducible E2a cell line for production of higher titer and safer adenoviral vectors. Virology *275*, 348-357.

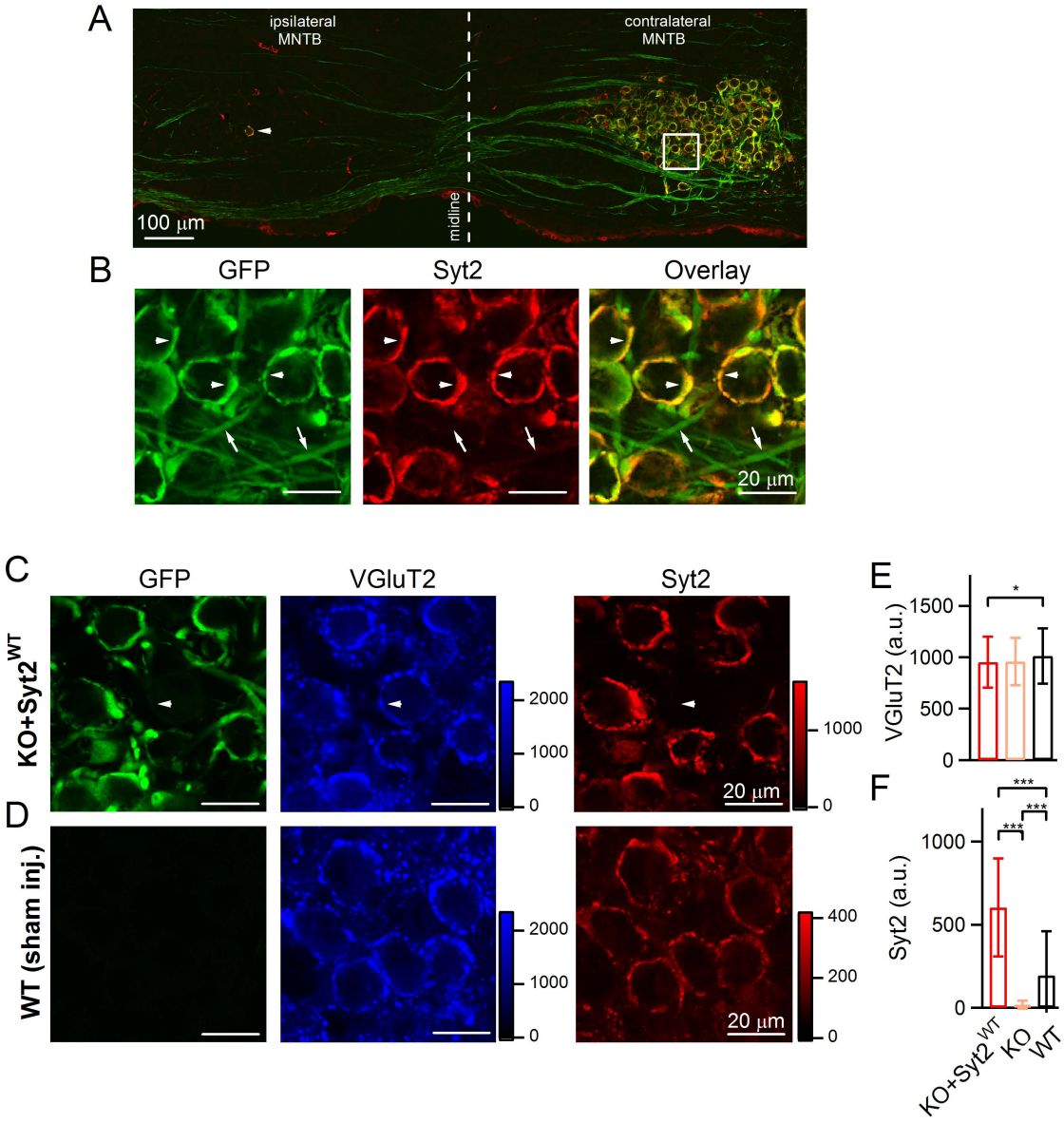
A
ipsilateral MNTB
contralateral MNTB
midline
100 µm
B
GFP
Syt2
Overlay
20 µm
C
GFP
VGluT2
Syt2
KO+Syt2WT
2000
1000
0
1000
0
20 µm
D
WT (sham inj.)
2000
1000
0
400
200
0
20 µm
E
VGluT2 (a.u.)
1500
1000
500
0
*
F
Syt2 (a.u.)
1000
500
0
***
***
***
KO+Syt2WT
KO
WT

Figure1

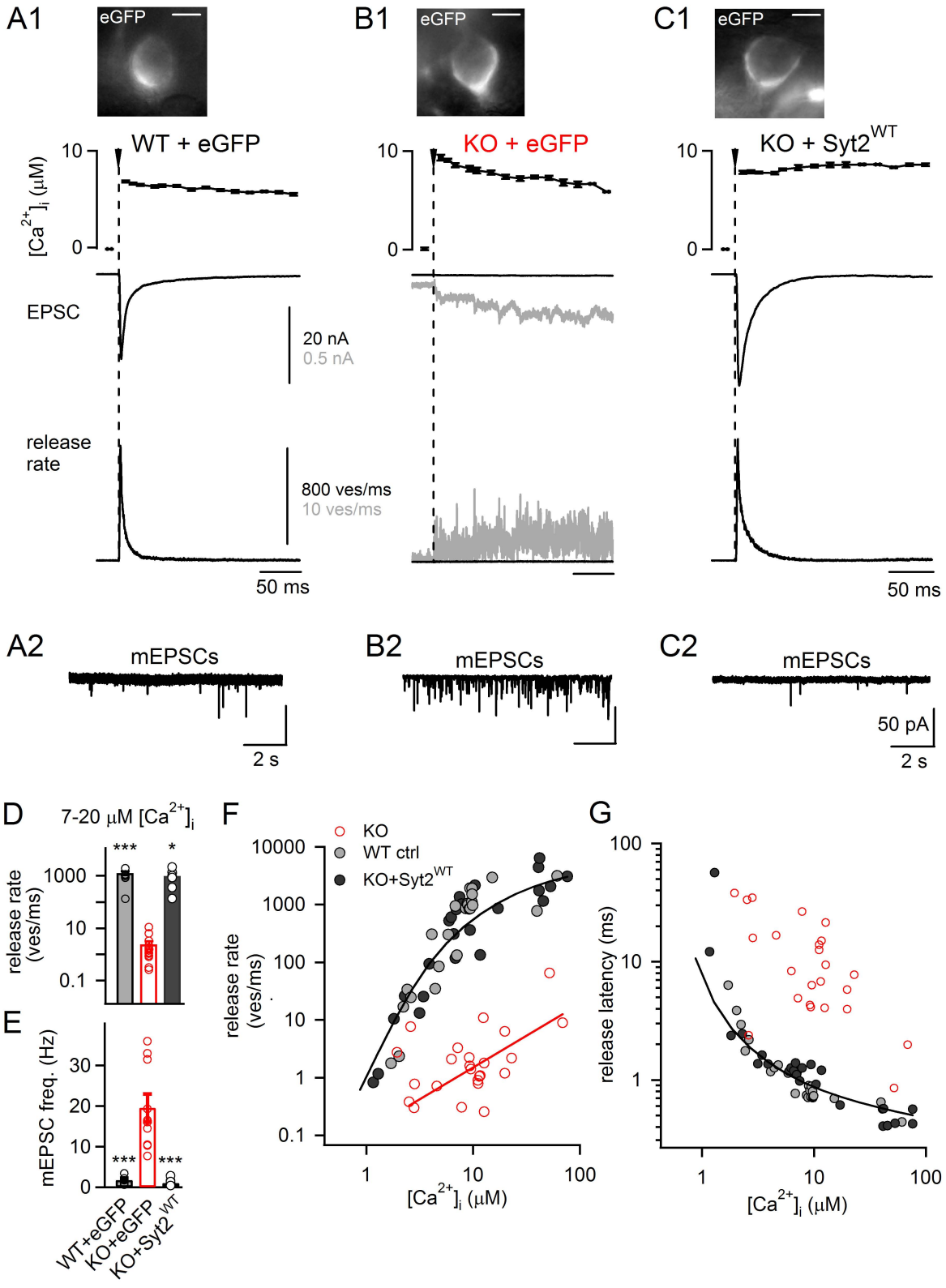
A1
eGFP
WT + eGFP
B1
eGFP
KO + eGFP
C1
eGFP
KO + Syt2WT
[Ca2+]i (μM)
10
0
EPSC
20 nA
0.5 nA
release rate
800 ves/ms
10 ves/ms
50 ms
50 ms
A2
mEPSCs
2 s
B2
mEPSCs
C2
mEPSCs
50 pA
2 s
D
7-20 μM [Ca2+]i
release rate (ves/ms)
1000
10
0.1
***
*
E
mEPSC freq. (Hz)
30
20
10
0
***
***
WT+eGFP
KO+eGFP
KO+Syt2 WT
F
KO
WT ctrl
KO+Syt2WT
release rate (ves/ms)
10000
1000
100
10
1
0.1
1
10
100
[Ca2+]i (μM)
G
release latency (ms)
100
10
1
1
10
100
[Ca2+]i (μM)

Figure 2

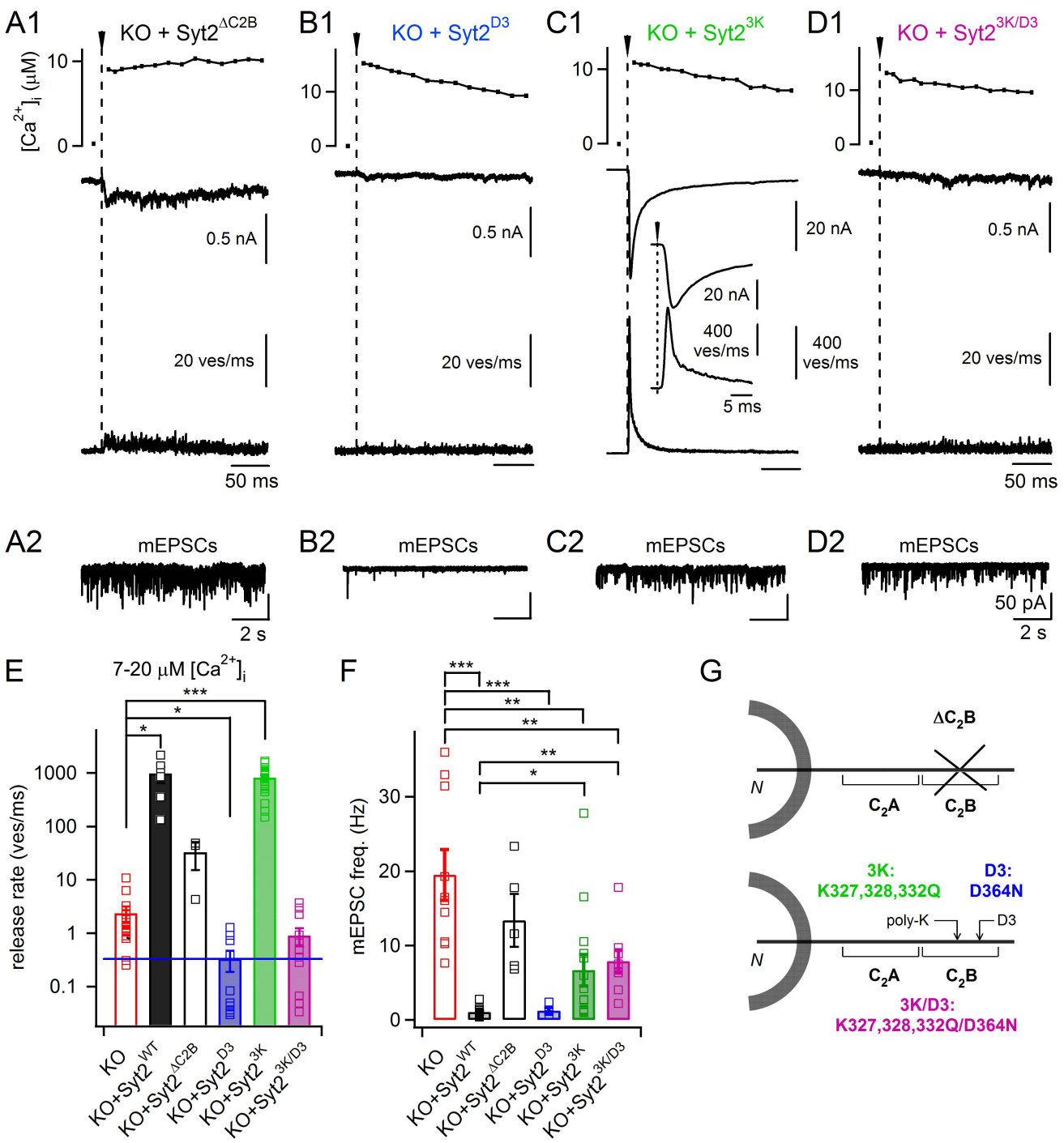
A1
KO + Syt2ΔC2B
B1
KO + Syt2D3
C1
KO + Syt2 3K
D1
KO + Syt2 3K/D3
[Ca2+]i (μM)
10
0
0.5 nA
20 ves/ms
50 ms
20 nA
400 ves/ms
5 ms
A2
mEPSCs
B2
C2
D2
2 s
50 pA
E
7-20 μM [Ca2+]i
release rate (ves/ms)
1000
100
10
1
0.1
KO
KO+Syt2 WT
KO+Syt2 ΔC2B
KO+Syt2 D3
KO+Syt2 3K
KO+Syt2 3K/D3
F
mEPSC freq. (Hz)
30
20
10
0
G
ΔC2B
N
C2A
C2B
3K:
K327,328,332Q
D3:
D364N
poly-K
D3
3K/D3:
K327,328,332Q/D364N

Figure 3

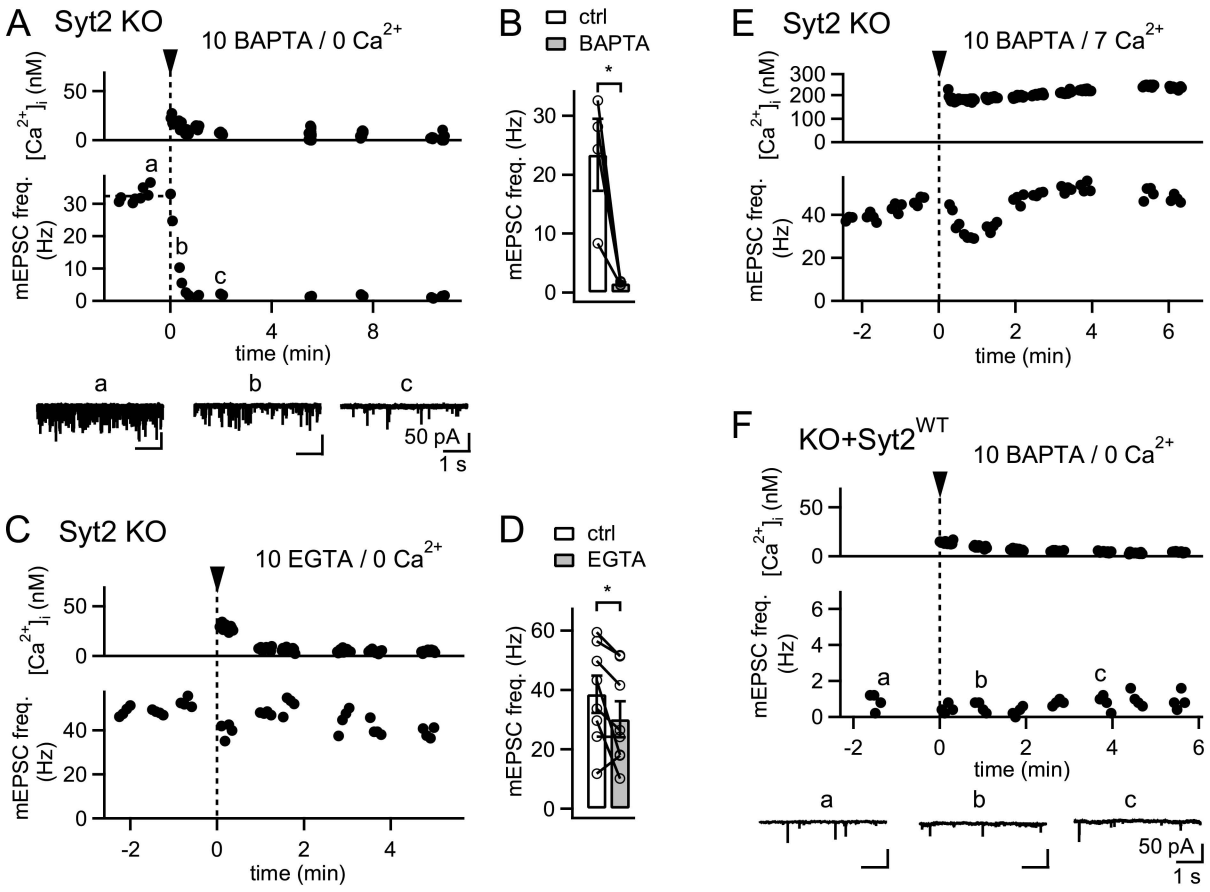
A
Syt2 KO
10 BAPTA / 0 Ca2+
[Ca2+]i (nM)
mEPSC freq. (Hz)
a
b
c
time (min)
50 pA
1 s
B
ctrl
BAPTA
mEPSC freq. (Hz)
C
Syt2 KO
10 EGTA / 0 Ca2+
D
ctrl
EGTA
E
Syt2 KO
10 BAPTA / 7 Ca2+
F
KO+Syt2WT
10 BAPTA / 0 Ca2+

Figure 4

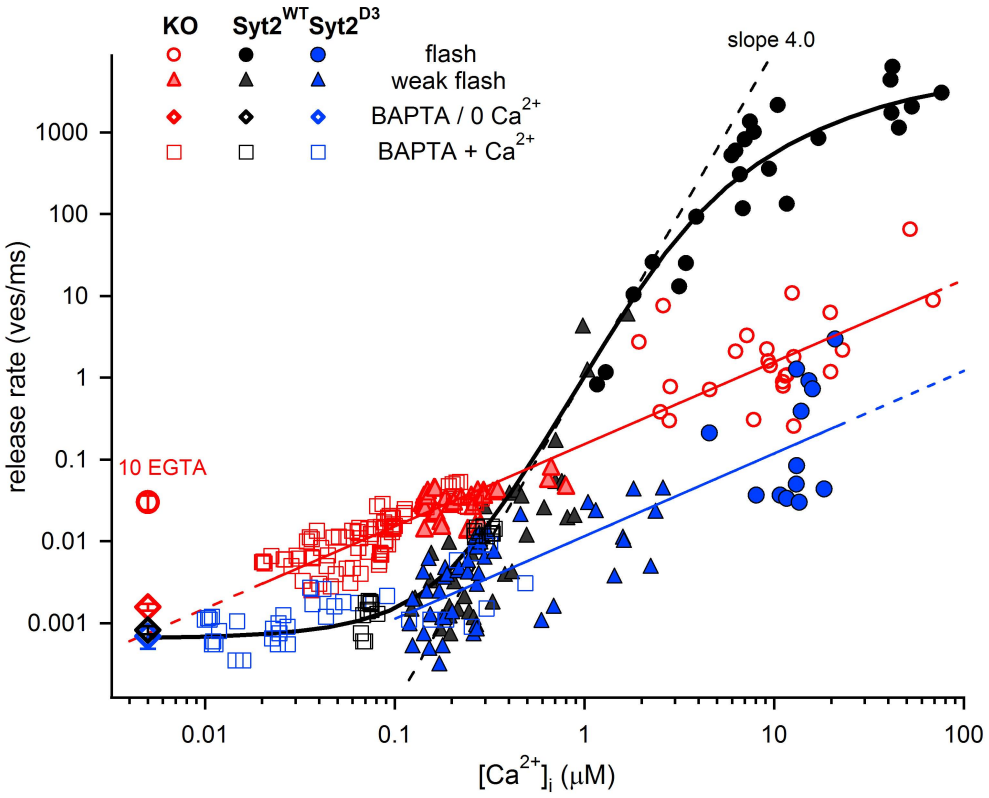
KO
Syt2WT
Syt2D3
flash
weak flash
BAPTA / 0 Ca2+
BAPTA + Ca2+
slope 4.0
10 EGTA
release rate (ves/ms)
1000
100
10
1
0.1
0.01
0.001
0.01
0.1
1
10
100
[Ca2+]i (µM)

Figure 5

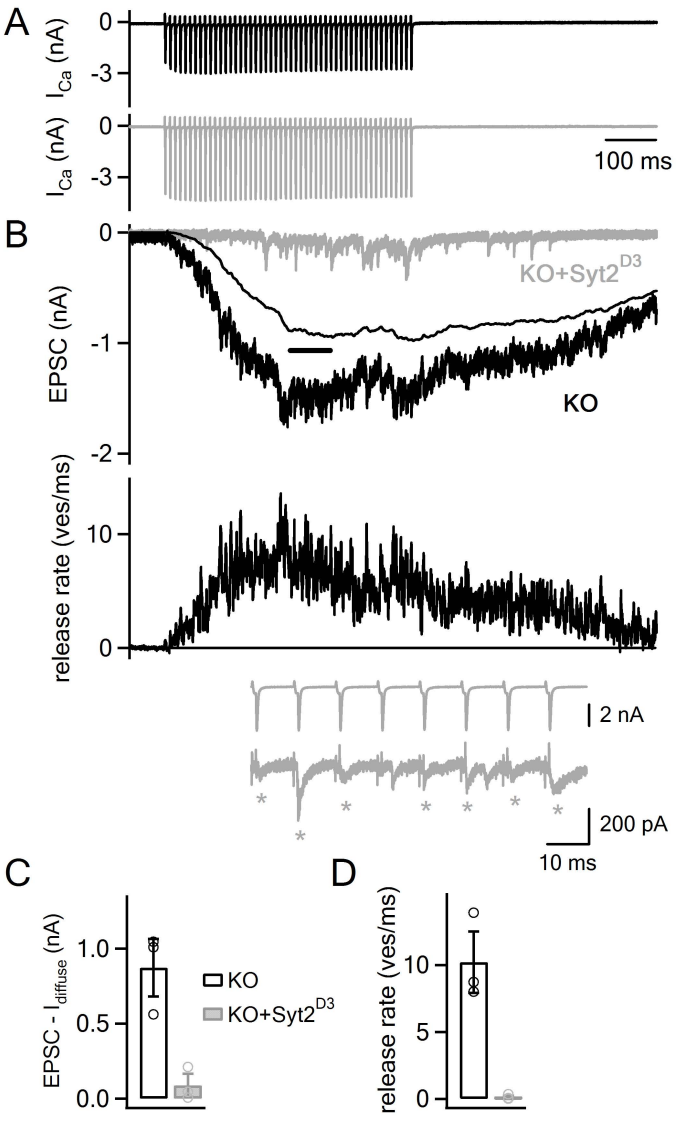
A
0
-3
I_{Ca} (nA)
0
-3
I_{Ca} (nA)
100 ms
B
0
-1
-2
EPSC (nA)
KO+Syt2^{D3}
KO
release rate (ves/ms)
10
0
2 nA
200 pA
10 ms
C
EPSC - $I_{diffuse}$ (nA)
1.0
0.5
0.0
KO
KO+Syt2^{D3}
D
release rate (ves/ms)
10
5
0

Figure 6

Supplemental Data

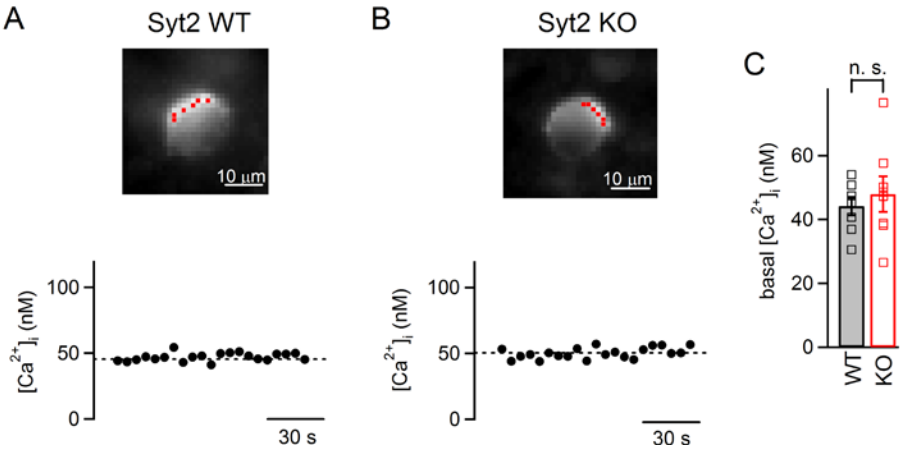

Figure S1. Basal $[Ca^{2+}]_i$ is not different in wild type and Syt2 KO calyx of Held synaptic terminals.

(A, B) To ask whether the increased mEPSC frequency in Syt2 -/- mice is caused by an enhanced $[Ca^{2+}]_i$ in the nerve terminal, we measured basal $[Ca^{2+}]_i$ in calyces of P12-P15 Syt2 +/+ (A) and Syt2 KO mice (B). Fura-2 (images at 380 nm excitation, *top panels*) was pre-loaded into the synaptic terminal via the patch pipette during a few minutes episode of whole-cell recording. In these experiments, the pipette solution was based on K-gluconate and contained no further Ca^{2+} buffers except fura-2 (50 µM). The extracellular solution included 1 µM TTX. After pre-loading, the pipette was carefully retracted, and fura-2 ratios were sampled for 5-10 minutes from six binned pixels (marked with red). The time course of basal $[Ca^{2+}]_i$ in these example cells (*bottom panels*) reported very similar values in wild type and Syt2 KO (45.4 and 50.3 µM average free $[Ca^{2+}]_i$ respectively, dotted lines).

(C) Summary of the basal $[Ca^{2+}]_i$ measurements showing no difference between wild type and Syt2 KO calyces of Held (average $[Ca^{2+}]_i$ of 44.2 ± 2.9 vs 47.9 ± 5.6 µM; p = 0.53, n = 8 cells in each group). Thus, the enhanced spontaneous release rate in Syt2 KO (see Figs. 2, 4-5) was not mediated by changes in the volume-averaged $[Ca^{2+}]_i$. Error bars = SEM.

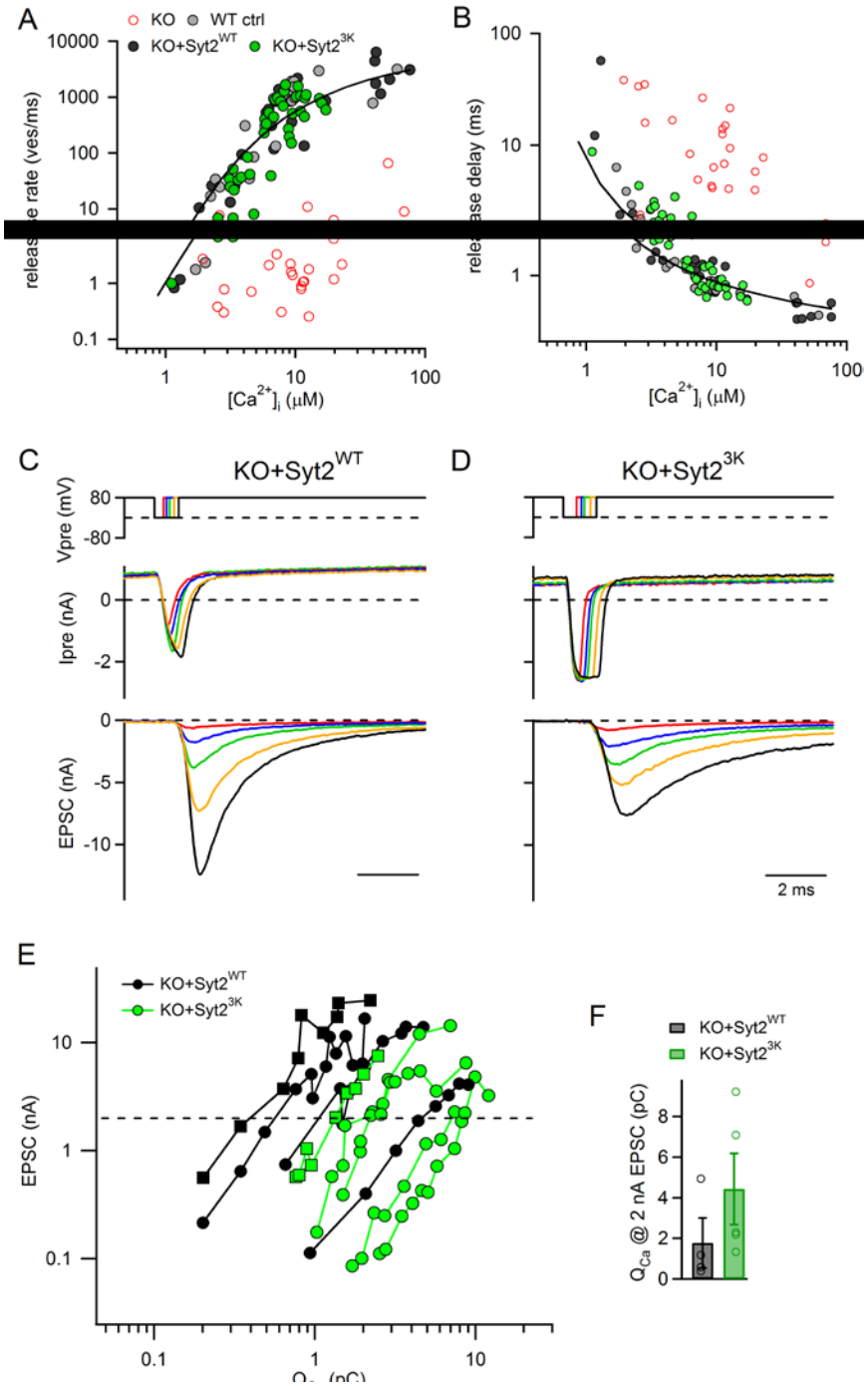

Figure S2. The Syt2^{3K} mutant efficiently rescued Ca^{2+}-uncaging evoked release but release evoked by brief Ca^{2+}-currents was impaired.

(A, B) The full $[Ca^{2+}]_i$ dependence of release rates (A) and release delays (B) for the rescue experiments with the Syt2^{3K} mutant shown in Fig. 3. In addition to the data for Syt2^{3K} mutant (green symbols), the corresponding data for the Syt2 KO, for the Syt2^{WT} rescue, and for the Syt2 wild-type control synapses were overlaid (re-plotted from Fig. 2F, G with the same

symbols). Note that the $Syt2^{K3}$ mutant led to full rescue of the Ca^{2+} - dependent release rate and release delays. However, we cannot exclude a small (~ 1.5 fold) slowing of the release kinetics in the range of 2 - 5 μM $[Ca^{2+}]_i$ as compared to the $Syt2^{WT}$ rescue data.

(C, D) Example experiments in $Syt2^{WT}$ rescue synapses (C), and $Syt2^{3K}$ mutant rescue synapses (D), in which release was evoked by inducing short Ca^{2+} influxes during presynaptic repolarisation from +80 to 0 mV for variable time intervals in double patch-clamp recordings (*top panels*). Note the absence of release at +80 mV presynaptic holding potential. Increasingly longer repolarizations to 0 mV evoked longer deflections in presynaptic currents (*middle panels*, I_{pre} traces were P/5 corrected), which in turn triggered larger EPSCs (*bottom panels*). Presynaptic Ca^{2+} influx (Q_{Ca}) was measured as an integral of only the negative component of the current (*middle panels*), assuming that the outward current offset originated from unblocked currents at +80 mV which were mostly absent at 0 mV. In the examples shown, a smaller Ca^{2+} influx in the $Syt2^{WT}$ rescue synapse (Q_{Ca} = 1.13 pC) could elicit a larger EPSC (12.3 nA, black traces in C) than the ~2.2 fold larger Q_{Ca} (2.47 pC) in the $Syt2^{3K}$ rescue synapse (EPSC of 7.54 nA, black traces in D).

(E) Plots of EPSC amplitudes plotted as a function of the corresponding Q_{Ca} in double-logarithmic coordinates for $Syt2^{WT}$ rescue synapses (black symbols) and $Syt2^{3K}$ rescue synapses (green symbols). The data were from the experiments described in (C, D); the example cells (C, D) are indicated by square symbols. Overall, the relations were rightward-shifted for the $Syt2^{3K}$ mutant, demonstrating a lower efficiency of brief presynaptic Ca^{2+} currents in triggering release.

(F) Ca^{2+} influx required to induce a given EPSC (measured as linearly interpolated Q_{Ca} value at the 2 nA level, dotted line in E) is higher in the $Syt2^{3K}$ than in $Syt2^{WT}$ rescue synapses (4.43 ± 1.75 pC, n = 5 cells vs 1.77 ± 1.23, n = 4 cells, respectively). Despite the clear trend in the data, the comparison did not reach statistical significance (p = 0.056, one-sided Mann-Whitney test). Nevertheless, the finding that an ~2 fold higher integral Ca^{2+} influx is needed

to evoke an EPSC of similar amplitude, together with the full rescue of Ca^{2+} uncaging – evoked release (panels A, B), indicate that the co-localization of vesicles and Ca^{2+} channel is likely compromised in the $Syt2^{3K}$ mutant (Young and Neher, 2009, and see Discussion). Error bars = SEM.

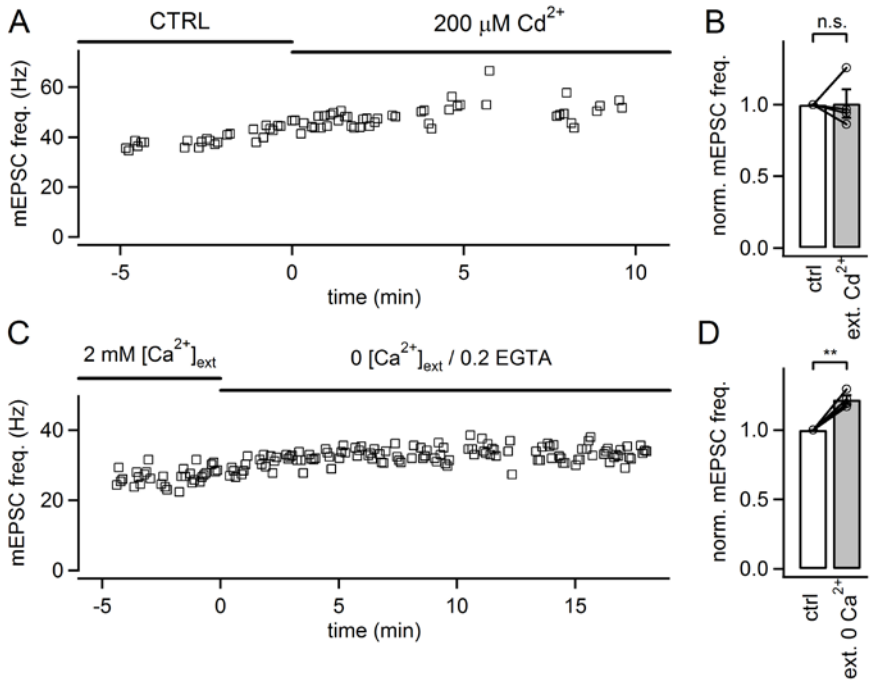

Figure S3. Spontaneous release at Syt2 KO calyces of Held could not be reduced by minimizing the possible influx of extracellular Ca^{2+}.

The different sensitivity of spontaneous release in Syt2 KO synapses to BAPTA (but not EGTA) indicates that short-lived $[Ca^{2+}]_i$ transients might cause spontaneous release in Syt2 KO synapses. To investigate whether these could be caused by spontaneous opening of Ca^{2+}-channels, we tested the effect of Cd^{2+}, and of removing extracellular Ca^{2+} on spontaneous release.

(A) Example time course of mEPSC frequency at a Syt2 KO calyx of Held synapse is shown, before (CTRL) and during the block of voltage-gated Ca-channels by 200 µM extracellular $CdCl_2$. Efficient action of Cd^{2+} was verified by monitoring the block of Ca^{2+} current in the postsynaptic MNTB cell (not shown); however, the mEPSC frequency did not decrease.

(B) Normalized mEPSC frequency following application of 200 µM Cd^{2+}. The change in mEPSC frequency was not significant ($p = 0.49$, paired t-test, $n = 4$).

(C) Frequency of mEPSCs in an example recording before and during the perfusion with a 0 Ca^{2+} / 200 µM EGTA external solution. There was no decrease in the mEPSC frequency, which instead slightly augmented. Efficient external Ca^{2+} washout was controlled by

monitoring the depolarization-evoked Ca^{2+} current in the MNTB neuron being recorded (not shown).

(D) Relative mEPSC frequency change upon removing external Ca^{2+}. There was a small but significant increase of the mEPSC frequency by ~ 22% upon Ca^{2+} removal ($p = 0.002$, paired t-test, n=4). Error bars = SEM.

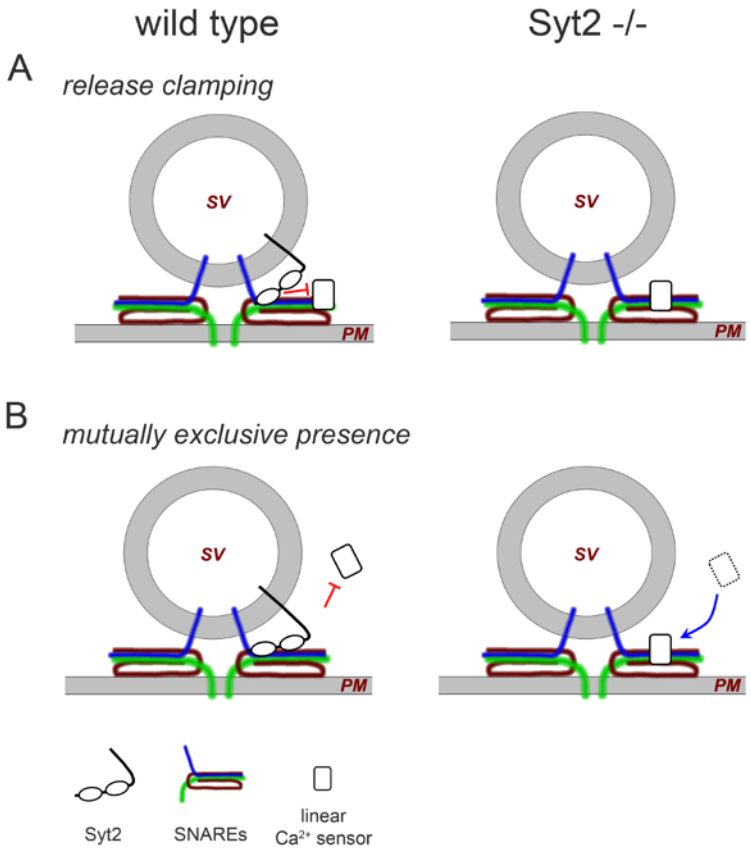

Figure S4. A scheme distinguishing two possible release clamping mechanisms of Syt2.

Two alternative scenarios are possible for the mechanism of release suppression by Syt2 in the wild type synapse. Syt2 could clamp the remaining Ca^{2+} sensor(s) by direct interaction, with both Ca^{2+} sensors present at the release machinery (A, *left*, *"release clamping model"*). Another explanation assumes that other Ca^{2+} sensor(s) can only access the release machinery in the absence of Syt2 (B, *"mutually exclusive presence"*). Our data from $Syt2^{3K}$ rescue (Figs 3, S2) favour the mechanism of clamping (A), because this mutant only weakly supported release clamping while it completely rescued the Ca^{2+} uncaging-evoked release. This supports the idea of a simultaneous presence of both Syt2 and the slow linear Ca^{2+} sensor(s) at the vesicle fusion machinery.

Supplemental Experimental Procedures

DNA cloning

The reverse primer to obtain ΔC_2B truncation mutant ($Syt2^{\Delta C2B}$) was 5'-CCCAAGCTTCTATCCGCCTTGTAGGTCTCTCCATTC-3' (underlined is the inserted stop codon). The mutagenesis primers to obtain D364N ($Syt2^{D3}$) and K327Q, K328Q, K332Q ($Syt2^{3K}$) constructs were 5'-GGTCGTCACCGTGCTAAACTATGACAAACTGGGC-3' and 5'-CAGCAGACGACGGTGCAGAAGAAGACCTTGAACCCCTACTTC-3', respectively; the mutated nucleotides are underlined. The combined K327Q, K328Q, K332Q/D364N ($Syt2^{3K/D3}$) mutation was obtained in two sequential steps using the same primers. All the primers were from Microsynth AG, Balgach, Switzerland.

Adenoviral vectors and adenovirus production

The modified 2nd generation adenoviral system was provided by Dr. Sam Young. It was constructed by modifications including, first, the removal of the E2a gene from the commercially available adenovirus genomic plasmid pBHGfrtΔE1,3FLP (AdMax, Microbix Biosystems Inc., Toronto, Canada) to generate ΔE1,2a,3 adenovirus as described (Zhou and Beaudet, 2000), and, second, the insertion of an eGFP expression cassette under the control of the human synapsin1 (hSyn) promoter (Kügler et al., 2003) into the E2a locus to allow eGFP co-expression along with a protein of interest (Young and Neher, 2009). The Syt2 rescue constructs, preceded by a Kozak consensus sequence 'GCCACC', were sub-cloned into the pDC511 shuttle vector (Microbix Biosystems Inc.) in between the hSyn promoter and the SV40 poly-adenylation signal. The genomic and shuttle plasmids were co-transfected into a packaging cell line E2T (Zhou and Beaudet, 2000), where the viral particles were generated and propagated. For the control experiments with eGFP expression alone, we used a 'dark' ΔE1,2a,3 genomic plasmid *without* eGFP in the E2a locus; instead, it was introduced by the

pDC511 shuttle vector encoding the eGFP sequence preceded by the hSyn promoter and the Kozak sequence. Adenovirus was propagated and plaque-purified in the E2T cell line (Zhou and Beaudet, 2000). Final purification and concentration of the viral particles was performed from the total lysate of ten 15-cm culture plates using the Vivapure AdenoPACK100RT kit (Sartorius Stedim Biotech, Aubagne, France). We used benzonase nuclease purchased separately from VWR or from Sigma, according to the manual for AdenoPACK kit. The viral preparation was concentrated into ~1 ml final volume of the injection buffer (in mM: 250 sucrose, 10 HEPES, 1 $MgCl_2$, pH 7.4) using Vivaspin 20 concentrators included in the kit. Purified virus was aliquoted and stored at -80°C before use. Viral titer, as measured by the OD_{260} method, was typically $1\text{-}5 \cdot 10^{12}$ particles/ml.

Stereotactic surgery

The mice were anaesthetized with 3% isoflurane (Minrad Inc., Buffalo, NY, USA) in O_2 and maintained at 1 - 1.5% isoflurane during the surgery using a custom-built gas mask and a Combi-vet gas anaesthesia system (Rothacher Medical GmbH, Bern, Switzerland). Lidocaine (2%) was used locally subcutaneously, and the body temperature was maintained with a homeothermic blanket (Harvard Aparatus, Holliston, MA, USA). The animal's head was mounted in the stereotactic instrument (model 940, Kopf Instruments, Tujunga, CA, USA) equipped with the mouse nose/tooth bar assembly (model 926-B) and non-rupture ear bars (model 922), the skin was cut open and the skull aligned with bregma and lambda being in one horizontal and transversal plane. Injections were performed through a craniotomy window made with a dental drill, using a vertical 34G steel needle (Coopers Needle Works Ltd, Birmingham, UK). Injections were done at three needle positions, located 1.67 mm lateral, and 0.65, 0.9 and 1.15 mm posterior from lambda, respectively. At each of these needle positions, the virus was injected at two 0.2 mm vertically-spaced depths with the

bottom level varying between 3.8 and 4.4 mm below the surface (i.e. injections were done at a total of six sites to improve the targeting of VCN).

Immunohistochemistry

After transcardial perfusion, the brains were dissected and post-fixed in 4% paraformaldehyde in PBS for 24 h at 4°C. The brains were then dehydrated in 30% w/v sucrose solution in PBS for 72 h at 4°C. The brainstem slices (30 μm) were cut from the frozen dehydrated brain on a Hyrax S30 sliding microtome (Carl Zeiss, Germany) equipped with a mounting platform immersed in a dry ice – ethanol bath. The sections were recovered and further processed in PBS, pH 7.4. Permeabilization and blocking was done in PBS supplemented with 5% horse serum (Invitrogen), 0.3% Triton X-100 (Sigma) and 0.2% BSA (AppliChem, Darmstadt, Germany). Primary anti-Syt2 and anti-VGluT2 antibodies were applied at 1:500 dilutions, and anti-GFP antibody was used at 1:1000 dilution in the staining solution (PBS supplemented with 2% horse serum, 0.15% Triton X-100 and 0.2% BSA) for 1 hour at room temperature with agitation. After triple washing in PBS, the secondary antibodies (1:200 dilutions in the staining solution) were incubated with the slices overnight at 4°C with agitation. The secondary antibodies used (all from Invitrogen) were donkey anti-mouse Alexa647 (A31571), goat anti-rabbit Alexa405 (A31556) and goat anti-chicken Alexa488 (A11039). Before mounting, the slices were triply washed in PBS, then once in ddH_2O, and mounted on the microscope slides using the Dako fluorescent mounting medium (Dako, Baar, Switzerland). Confocal images were captured on an inverted Leica SP2 microscope (Leica Microsystems, Wetzlar, Germany) equipped with the HCX PL APO 40x/1.25 NA oil immersion objective using the 405, 488 and 633 nm laser lines for excitation. The lateral pixel dimension was typically 96 nm. In quantitative immunofluorescence analysis (Fig. 1C-F), the samples were processed in parallel, and confocal images were acquired during a single imaging session with identical imaging settings avoiding saturation of detectors.

Slice preparation and electrophysiology

A bicarbonate-buffered solution for incubation of slices and for use as an extracellular recording solution contained (in mM): 125 NaCl, 25 $NaHCO_3$, 2.5 KCl, 1.25 NaH_2PO_4, 25 glucose, 0.4 ascorbic acid, 3 myo-inositol, 2 Na-pyruvate, 2 $CaCl_2$ and 1 $MgCl_2$ (pH 7.4, when bubbled with 95% O_2 / 5% CO_2). Presynaptic calyces and postsynaptic principal MNTB neurons were visually identified under upright microscope BX51WI (Olympus, Tokyo, Japan) with a 60x/0.9 NA water immersion objective (Olympus), equipped with Dodt gradient contrast illumination (Luigs and Neumann, Ratingen, Germany) and an Imago CCD camera (TILL Photonics, Gräfelfing, Germany). GFP expression at the calyces was checked at 470 nm excitation light from Polychrome V monochromator (TILL Photonics) using a 500 nm long-pass dichroic mirror and an eGFP+IR emission filter (AHF analysentechnik, Tübingen, Germany). The postsynaptic pipette solution contained (in mM): 135 Cs-gluconate, 20 TEA, 10 HEPES, 5 Na_2-phosphocreatine, 4 MgATP, 0.3 Na_2GTP, 5 Cs-EGTA, pH 7.2. Postsynaptic currents were normally recorded at -70 mV and corrected off-line for residual uncompensated series resistance (R_s typically was 3 - 8 MΩ, compensated up to 85%). In some cases, to avoid amplifier saturation by EPSCs > 20 nA, the holding potential was set in a range from -50 to -30 mV, followed by off-line linear scaling of the EPSC assuming a reversal potential of 0 mV for AMPA-mediated EPSCs.

Ca^{2+} uncaging and Ca^{2+} imaging

The presynaptic intracellular solutions contained as a basis (in mM): 130 Cs-gluconate, 20 TEA-Cl, 20 HEPES, 5 Na_2-phosphocreatine, 5 Na_2ATP, 0.3 Na_2GTP, 0.5 $MgCl_2$, pH 7.2, which was supplemented with Ca^{2+}-indicator fura-2FF and Ca^{2+}-loaded DM-Nitrophen as described in the Experimental Procedures. An SP-20 flash lamp with SP395 filter (Rapp OptoElectronic, Hamburg, Germany) produced short UV flashes to induce Ca^{2+} uncaging. Fura-2FF fluorescence was excited at 350 and 380 nm using Polychrome V monochromator

and imaged with an Imago CCD camera (TILL Photonics). For small $[Ca^{2+}]_i$ steps (< 1 μM, Fig. 5, 'weak flash'), 2 DM-Nitrophen/1.75 $CaCl_2$ containing solution was used in combination with 0.2 mM fura-2 (Invitrogen), and the flash lamp and monochromator light intensities were attenuated by 68 - 95% using ND filters, to reduce the uncaging efficiency during the main flash and during the following fura-2 imaging series. Fura dyes used for the determination of post-flash $[Ca^{2+}]_i$ were calibrated for each condition as described in (Schneggenburger, 2000).

Data analysis

Multivariate fit of Ca^{2+}-dependent release parameters with a prediction by a single-pool allosteric model for Ca^{2+} binding and transmitter release (Lou et al., 2005; see Figs. 2F,G, 5, S2; black fit lines) were done in IgorPro as described in (Kochubey et al., 2009), resulting in the parameters as follows: k_{on} = 1.4e8 $s^{-1}M^{-1}$, k_{off} = 2.5e3 s^{-1}, b = 0.49, l_+ = 3.5e-4 s^{-1}, f = 25 with an average pool size of 1820 ves, as estimated from the uncaging experiments in $Syt2^{WT}$ rescue cells.

Supplemental references

Schneggenburger, R. (2000). Ca^{2+} uncaging in nerve terminals. In Imaging neurons : a laboratory manual, R. Yuste, F. Lanni, and A. Konnerth, eds. (Cold Spring Harbor, N.Y., Cold Spring Harbor Laboratory Press), pp. 415-419.